The Company of Biologists

RESEARCH ARTICLE

The single *Marchantia polymorpha FERONIA* homolog reveals an ancestral role in regulating cellular expansion and integrity

Martin A. Mecchia[1,§], Moritz Rövekamp[1,*,§], Alejandro Giraldo-Fonseca[1], Dario Meier[1], Philippe Gadient[1,‡], Hannes Vogler[1], Daria Limacher[1], John L. Bowman[2] and Ueli Grossniklaus[1,¶]

ABSTRACT

Plant cells are surrounded by a cell wall, a rigid structure that is not only important for cell and organ shape, but is also crucial for intercellular communication and interactions with the environment. In the flowering plant *Arabidopsis thaliana*, the 17 members of the *Catharanthus roseus* RLK1-like (*Cr*RLK1L) receptor kinase family are involved in a multitude of physiological and developmental processes, making it difficult to assess their primary or ancestral function. To reduce genetic complexity, we characterized the single *Cr*RLK1L gene of *Marchantia polymorpha*, Mp*FERONIA* (Mp*FER*). Plants with reduced Mp*FER* levels show defects in vegetative development, i.e. rhizoid formation and cell expansion, and have reduced male fertility. In contrast, cell integrity and morphogenesis of the gametophyte are severely affected in Mp*fer* null mutants and Mp*FER* overexpression lines. Thus, we conclude that the *Cr*RLK1L gene family originated from a single gene with an ancestral function in cell expansion and the maintenance of cellular integrity. During land plant evolution, this ancestral gene diversified to fulfill a multitude of specialized physiological and developmental roles in the formation of both gametophytic and sporophytic structures essential to the life cycle of flowering plants.

KEY WORDS: Cell wall integrity, Cell elongation, *Cr*RLK1L receptor kinases, *Marchantia polymorpha*, Signaling pathway evolution

INTRODUCTION

The functioning of plant cells is contingent upon the cell wall acting as a barrier between the cell and its environment. This complex matrix of polysaccharides, glycoproteins and other organic compounds defines the growth and shape of a cell and provides protection against biotic and abiotic stresses (Zhu et al., 2021; Showalter, 1993; Franck et al., 2018). Moreover, the cell wall has to resist turgor pressure while also allowing cell expansion during growth. Thus, sensing and controlling cell wall integrity (CWI) is crucial for plant cells, and receptor kinases (RKs) play an important role in sensing extracellular cues that activate intracellular pathways. Different RK subfamilies are defined by their extracellular domain (ECD), which is more variable than their

transmembrane and kinase domains (Shiu and Bleecker, 2001). Over the last decade, the *Catharanthus roseus* RLK1-like (*Cr*RLK1L) subfamily emerged as important CWI sensors (Steinwand and Kieber, 2010; Wolf et al., 2012).

Functions have been assigned to 15 of the 17 *Cr*RLK1L members encoded in the *Arabidopsis thaliana* genome: they are required for sensing environmental cues and cell-cell communication in diverse contexts, including reproduction, hormone signaling, cell expansion, innate immunity and various stress responses (Escobar-Restrepo et al., 2007; Hématy et al., 2007; Boisson-Dernier et al., 2009; Guo et al., 2009a,b; Kessler et al., 2010; Bai et al., 2014; Schoenaers et al., 2018; Miyazaki et al., 2009; Keinath et al., 2010; Duan et al., 2010; Galindo-Trigo et al., 2020; Zhu et al., 2018; Li et al., 2015; Richter et al., 2017, 2018; Stegmann et al., 2017). For instance, *FERONIA* (At*FER*), *THESEUS1* (At*THE1*), *HERCULES1* (At*HERK1*) and At*HERK2* are required for cell elongation as At*fer* single, At*the1* At*herk1* double, and At*the1* At*herk1* At*herk2* triple mutants exhibit stunted growth (Hématy et al., 2007; Guo et al., 2009a,b; Kessler et al., 2010). Root hairs burst in mutants in which At*FER* and [Ca²⁺]*cyt*-*ASSOCIATED PROTEIN KINASE1* (At*CAP1*) [also known as *ERULUS* (At*ERU*)] are affected (Bai et al., 2014; Duan et al., 2010). Moreover, At*FER* plays a role in powdery mildew resistance (Kessler et al., 2010), innate immunity (Keinath et al., 2010; Stegmann et al., 2017), calcium signaling (Ngo et al., 2014), phytohormone signaling (Guo et al., 2009b; Yu et al., 2012; Mao et al., 2015; Deslauriers and Larsen, 2010), and mechano- and heavy metal sensing (Richter et al., 2017; Shih et al., 2014). In most contexts, the *Cr*RLK1Ls tend to promote cellular growth and cell elongation. In contrast, At*THE1* actively inhibits cell elongation in hypocotyls when cell wall perturbations occur, e.g. as a result of mutations in the cell wall biosynthesis machinery or upon treatment with isoxaben, a cellulose synthesis inhibitor (Hématy et al., 2007; Denness et al., 2011).

In addition to regulating cellular growth during the vegetative phase of the life cycle, several *Cr*RLK1Ls play a role during fertilization by controlling the growth and reception of the pollen tube. In the female gametophyte, At*FER* is highly expressed in the two synergid cells that flank the egg cell and are important for double fertilization (Escobar-Restrepo et al., 2007; Okuda et al., 2009). At*FER* is crucial for pollen tube reception and the release of the two sperm cells (Escobar-Restrepo et al., 2007; Guo et al., 2009b; Ngo et al., 2014; Huck et al., 2003; Rotman et al., 2003), a process also involving two other, redundantly acting synergid-expressed *Cr*RLK1Ls, At*HERK1* and *ANJEA* (At*ANJ*) (Galindo-Trigo et al., 2020). Moreover, At*FER* and At*ANJ* also play a role in pollen-stigma recognition during pollen germination (Zhu et al., 2021). In contrast to these synergid-expressed *Cr*RLK1Ls, four pollen-expressed *Cr*RLK1Ls, named *ANXUR1* (At*ANX1*), At*ANX2*, *BUDDHAS PAPER SEAL1* (At*BUPS1*) and At*BUPS2* (Boisson-Dernier et al., 2009; Miyazaki et al., 2009;

[1]Department of Plant and Microbial Biology and Zurich-Basel Plant Science Center, University of Zurich, 8008 Zurich, Switzerland. [2]The School of Biological Sciences, Monash University, Clayton, Melbourne, Victoria 3800, Australia.
*Present address: Kantonsschule Uetikon am See, 8708 Uetikon am See, Switzerland. ‡Present address: Institute of Molecular Plant Science, University of Edinburgh, Daniel Rutherford Building, Max Born Crescent, Edinburgh EH9 3BF, UK.
§These authors contributed equally to this work

¶Author for correspondence (grossnik@botinst.uzh.ch)

M.A.M., 0000-0002-3444-3294; M.R., 0000-0001-6989-9104; A.G.-F., 0000-0001-7251-8245; H.V., 0000-0002-6552-4708; J.L.B., 0000-0001-7347-3691; U.G., 0000-0002-0522-8974

DEVELOPMENT

1

Zhu et al., 2018; Ge et al., 2017), are redundantly required for pollen tube integrity and tip growth.

To transduce extracellular cues, *Cr*RLK1Ls bind secreted peptides of the RAPID ALKALINIZATION FACTOR (RALF) family (Stegmann et al., 2017; Ge et al., 2017; Haruta et al., 2014; Dünser et al., 2019; Xiao et al., 2019), which induce complex formation with members of LORELEI (LRE) family of GPI-anchored proteins to signal to the interior of the cell (Ge et al., 2017; Xiao et al., 2019; Mecchia et al., 2017; Capron et al., 2008). Hence, it was suggested that at least some *Cr*RLK1Ls act as CWI sensors that coordinate cell elongation in response to changes in the cell wall (Boisson-Dernier et al., 2011; Hématy and Höfte, 2008; Cheung and Wu, 2011; Nissen et al., 2016; Feng et al., 2018; Lindner et al., 2012). A role as CWI sensors is also consistent with recent findings that AtFER interacts with pectin (Feng et al., 2018; Tang et al., 2021; Lin et al., 2021).

The 17 *A. thaliana Cr*RLK1Ls act partially redundantly and sometimes even have opposite effects on cellular growth (reviewed by Li et al., 2015; Nissen et al., 2016; Lindner et al., 2012; Galindo-Trigo et al., 2016). To investigate the original function of *Cr*RLK1Ls, we characterized them in a system with reduced genetic complexity: the liverwort *Marchantia polymorpha*, the genome of which encodes only one *Cr*RLK1L (Bowman et al., 2017; Rövekamp et al., 2014). Liverworts represent an early diverging land plant lineage and have been hypothesized to retain, at least in part, characteristics of the earliest land plants (Bowman et al., 2017, 2007; Nishiyama et al., 2003; Qiu et al., 2006; Wickett et al., 2014; Mishler and Churchill, 1984; Kenrick and Crane, 1997). The presence of similar types of gene families in all plant lineages suggests that the differences in development evolved by co-opting and modifying existing developmental programs and genetic networks, rather than through the evolution of novel genes (Bowman et al., 2007; Nishiyama et al., 2003; Floyd and Bowman, 2007). *M. polymorpha* is thus an ideal system in which to study the ancestral role of genes and how it was modulated and diversified during land plant evolution (Bowman et al., 2017, 2016; Ishizaki, 2017).

We refer to the single *Cr*RLK1L encoded in the *M. polymorpha* genome, Mp4g15890 (Mapoly0869s0001), as Mp*FERONIA* (Mp*FER*) (Galindo-Trigo et al., 2016; Bowman et al., 2017; Rövekamp et al., 2014) [also known as Mp*THESEUS* (Mp*THE*)] (Honkanen et al., 2016). An Mp*fer* mutant was identified in a large T-DNA screen for defective rhizoid formation, developing short and irregularly shaped rhizoids with brown tips, indicating rhizoid rupture (Honkanen et al., 2016). In the same screen, a mutant affecting the ortholog of the *A. thaliana* receptor-like cytoplasmic kinase *MARIS* (At*MRI*), known to act downstream of At*FER*, was identified with a similar phenotype [named Mp*mri* or Mp*pti*; Mp7g17560 (Mapoly0051s0094)] (Honkanen et al., 2016; Westermann et al., 2019). As in *A. thaliana*, a dominant active version of Mp*MRI* can partially rescue the Mp*fer* rhizoid phenotype (Westermann et al., 2019). This suggests that at least some of the machinery associated with cell elongation and CWI sensing is conserved between *A. thaliana* and *M. polymorpha*.

Here, we report that Mp*FER* function is required for a variety of aspects of *M. polymorpha* gametophyte development. Phylogenetic analyses suggest that *Cr*RLK1L genes first appeared in the common ancestor of land plants. The characterization of lines with reduced Mp*FER* levels indicates that, in addition to its function in rhizoid formation, Mp*FER* controls cell size and organ growth and is involved in male gametogenesis and fertility. Analysis of the Mp*FER* expression pattern points to an involvement in female sexual organogenesis and sporophyte development. Our data suggest that the broad involvement of *Cr*RLK1L function in the development and physiology of land plants is an ancestral and conserved characteristic, although the functions of *Cr*RLK1Ls were extended and adapted to control additional developmental processes in the sporophyte during the course of land plant evolution.

RESULTS
*Cr*RLK1L is conserved in land plants and arose in this lineage
The *M. polymorpha* genome encodes a single *Cr*RLK1L homolog [Mp4g15890 (Mapoly0869s0001)] (Galindo-Trigo et al., 2016; Bowman et al., 2017; Rövekamp et al., 2014). Like other *Cr*RLK1L members, this gene encodes an intracellular serine/threonine kinase domain, a transmembrane domain and an extracellular malectin-like domain with two malectin domains (Fig. 1A). Given that the ECD of *Cr*RLK1Ls in *A. thaliana* is crucial for their function and, in contrast to the kinase domain, not interchangeable (Kessler et al., 2014), we performed a phylogenetic analysis with the amino acid sequences of the predicted malectin-like domain of Mp4g15890, the *Cr*RLK1Ls of the mosses *Physcomitrium patens* (five members), *Sphagnum fallax* (seven members) and *Ceratodon purpureus* (three members), the hornworts *Anthoceros agrestis* Bonn (one member), *Anthoceros agrestis* Oxford (one member) and *Anthoceros punctatus* (one member), the lycophyte *Selaginella moellendorffii* (two members), the basal angiosperm *Amborella trichopoda* (nine members) and the 17 *Cr*RLK1Ls of *A. thaliana* (Fig. 1B). The *M. polymorpha Cr*RLK1L member grouped together with the *Cr*RLK1Ls of basal land plants and was in the same clade as, for example, AtFER, AtHERK2 and AtANX1/2, whereas AtTHE1 was in a different one (Fig. 1B). Based on this phylogenetic position and the fact that the malectin-like domain of the *M. polymorpha Cr*RLK1L shared the highest amino acid identity with AtFER (Fig. S1A), we named it MpFER (Bowman et al., 2017; Rövekamp et al., 2014; Westermann et al., 2019).

Interestingly, no significant similarity to the MpFER malectin-like domain was found among available genomic data of six Chlorophyte algae (*Chlamydomonas reinhardtii*, *Dunaliella salina*, *Volvox carteri*, *Coccomyxa subellipsoidea*, *Micromonas pusilla*, *Ostreococcus lucimarinus*) and expression data of six Charophycean algae (*Klebsormidium nitens*, *Nitella mirabilis*, *Coleochaete orbicularis*, *Spirogyra pratensis*, *Mesostigma viride*, *Closterium peracerosum–strigosum–littorale* complex). In the *Closterium* complex, an RK named CpRLK1 expressed during sexual reproduction was suggested to be a *Cr*RLK1L homolog (Hirano et al., 2015). However, comparing the full sequence or the ECD of CpRLK1 with the predicted *M. polymorpha* proteome, higher identity to another RK was found [Mp1g17720 (Mapoly0001s0111)] (Fig. S1B,C). Moreover, no RALF orthologs have been reported in algae, suggesting the origin of the *Cr*RLK1L pathway in land plants (Bowman et al., 2017). A similar conclusion was recently reached by analyzing the RALF family in *P. patens* (Ginanjar et al., 2021). Moreover, the best candidate obtained by BLAST analysis using the MpFER malectin-like domain against the genome of the Charophycean alga *Chara braunii* clustered outside the *Cr*RLK1L phylogenetic tree (Fig. 1B, Fig. S1B).

To support MpFER as a member of the *Cr*RLK1L subfamily, the 3D structure of its ECD was modeled (Schwede et al., 2003) using the structure of the AtFER ECD (PDB 6a5b.1A; Xiao et al., 2019) as a template (Fig. 1C). Overall, the predicted structure of the MpFER ECD is highly similar to that of AtFER, keeping an almost identical number of secondary structures [seven α-helices and 33 β-sheets in the MpFER ECD (Xiao et al., 2019) and eight α-helices and 34 β-sheets in the AtFER ECD, respectively], and a similar spatial disposition for 32 of the β-sheet structures and six of the
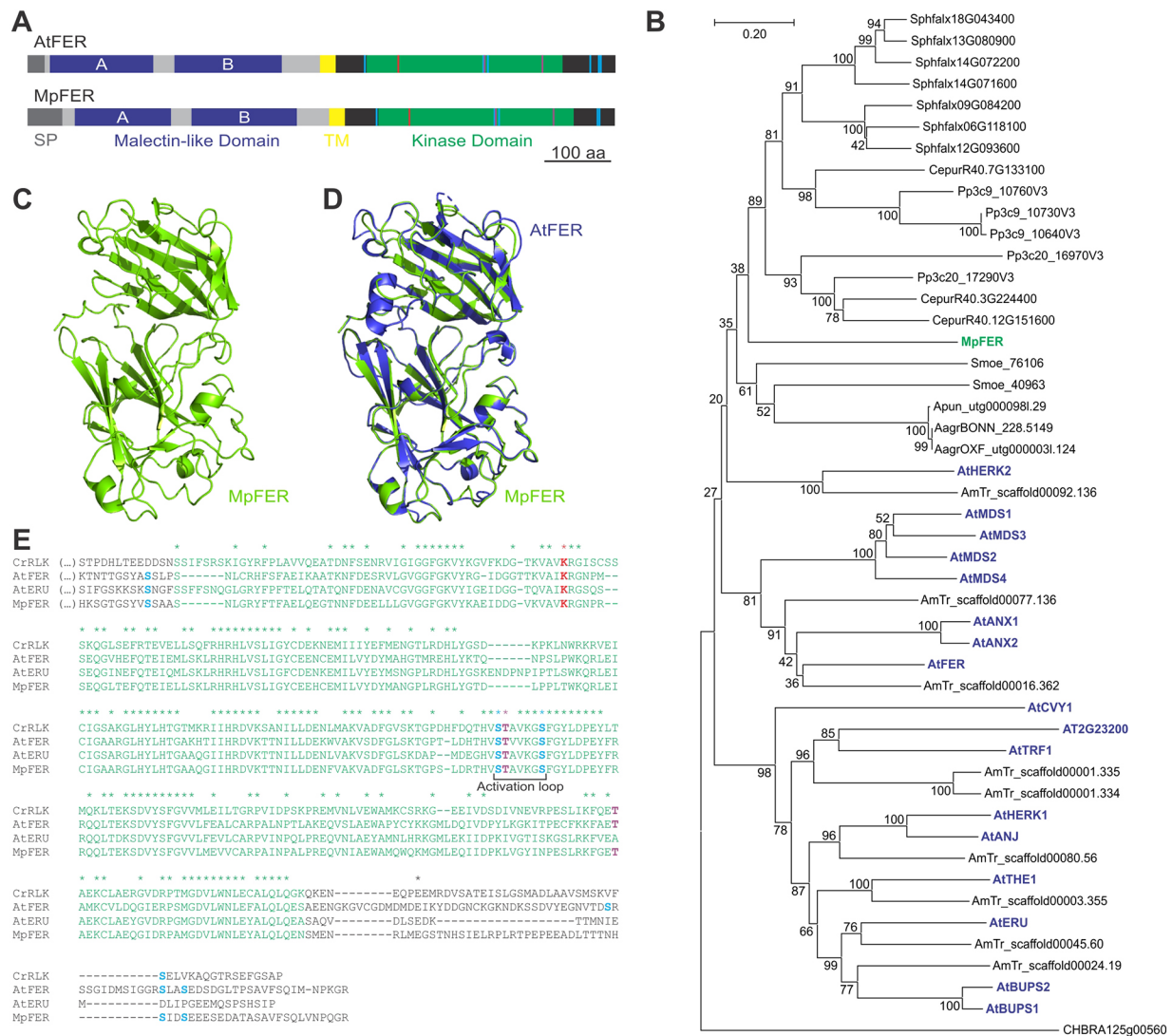
Fig. 1. *Cr*RLK1Ls are conserved among land plants. (A) Representation of AtFER and MpFER proteins. The malectin domains are represented in blue and kinase domains in green. SP, signal peptide; TM, transmembrane domain (yellow). Amino acids important for regulation and activity are marked in red, violet and light blue as described in E. (B) A rooted neighbor-joining tree of the amino acid sequence of the predicted malectin-like domain (corresponding to aa 76-431 of MpFER). *Cr*RLK1L members from *Marchantia polymorpha* (Mp, green), *Physcomitrium patens* (Pp), *Sphagnum fallax* (Sphfalx), *Ceratodon purpureus* (Cepur), *Anthoceros agrestis* Bonn (AagrBONN), *Anthoceros agrestis* Oxford (AagrOXR), *Anthoceros punctatus* (Apun), *Selaginella moellendorffii* (Smoe), *Amborella trichopoda* (AmTr) and *Arabidopsis thaliana* (At, blue) were used. The best hit from *Chara braunii* (CHBRA) was also included. The numbers indicate the bootstrap values (%) from 1000 replications. The given scale represents a substitution frequency of 0.1 amino acids per site. (C) Schematics of the predicted 3D structure of the MpFER malectin-like domain, showing predicted α-helix and β-sheet structures. (D) Structural superposition of the malectin-like domains of AtFER (blue) and MpFER (green). (E) Alignment of the cytoplasmic domains of MpFER, AtERU, AtFER and *Cr*RLK1 (CRLK). Kinase domains are in green, putative phosphorylation sites in light blue (Ser) and violet (Thr), and the conserved catalytic Lys in red. See also Fig. S1.

α-helices (Fig. 1C). When comparing the structural superposition of the AtFER and MpFER ECDs (Fig. 1D, Fig. S1D), we observed that most conserved parts of the malectin-like domain are in the core of the protein, and the more variable parts are located peripherally. Moreover, the 3D structure of the CpRLK1 ECD could not be properly modeled using the AtFER ECD (Fig. S1D,E), and neither could that of *C. braunii* (Fig. S1D,F). Taken together, these results suggest that the malectin-like domain of MpFER could interact with similar proteins as AtFER does in *A. thaliana* and may thus be involved in similar pathways. Sequence comparison of the MpFER kinase domain showed conservation of the activation loop and a Lys residue important for catalytic activity (Fig. 1E). Furthermore, several determined phosphorylation sites found in AtFER, AtERU and CrRLK1 were conserved in MpFER (Fig. 1E) (Schoenaers

et al., 2018; Haruta et al., 2014; Liu et al., 2016; Schulze-Muth et al., 1996). Given that the genomes of *M. polymorpha* and *Anthoceros* spp. encode a single *Cr*RLK1L and this RK family is not present in Charophycean algae, we propose MpFER to be basal and orthologous to all other land plant *Cr*RLK1Ls, and that the *Cr*RLK1L family arose as plants conquered land.

Mp*FER* is broadly expressed throughout the *M. polymorpha* life cycle

In *A. thaliana*, the expression patterns of the 17 *Cr*RLK1L members span vegetative and reproductive stages and both generations of the life cycle (reviewed by Lindner et al., 2012), pointing to the importance of *Cr*RLK1Ls for basic cellular functions. To assess whether this pattern is reflected in the land plant with the most

ancestral characteristics, a promoter fragment of 3.2 kb ($_{pro}$MpFER) was used to drive expression of a triple yellow fluorescent protein (trpVNS) with a nuclear localization signal ($_{pro}$MpFER:trpVNS) and transformed into *M. polymorpha* sporelings. All transformants expressing the trpVNS fluorescent protein (45 of 48 independent lines) exhibited an indistinguishable expression pattern (Fig. 2). During vegetative stages of gametophyte development, expression was observed in most cells of the thallus (Fig. 2A,B). In concordance with the importance of MpFER for rhizoids (Honkanen et al., 2016), high trpVNS expression was observed in these tip-growing cells (Fig. 2A′,B′). Although trpVNS was expressed in gemma cups, no expression was observed in mature gemmae (clonal, asexual propagules produced in the gemma cups), possibly owing to their dormancy (Fig. 2C,D).

In mature female sexual organs, strong expression was observed in the entire archegoniophore (Fig. 2E,F). The archegonia expressed trpVNS in most cells, except for the egg cell (Fig. 2G). However, after fertilization, $_{pro}$MpFER:trpVNS became active in the zygote (Fig. 2H). In male sexual organs, trpVNS was broadly detected in the antheridial splash platform (Fig. 2I,J) and, specifically, in the spermatogenous tissue of the antheridia and the non-reproductive jacket cells surrounding them at different developmental stages (Fig. 2K). Inside the sporogonium, the sporogenous cells, and subsequently the developing spores, but not the elater cells, strongly expressed trpVNS (Fig. 2L).
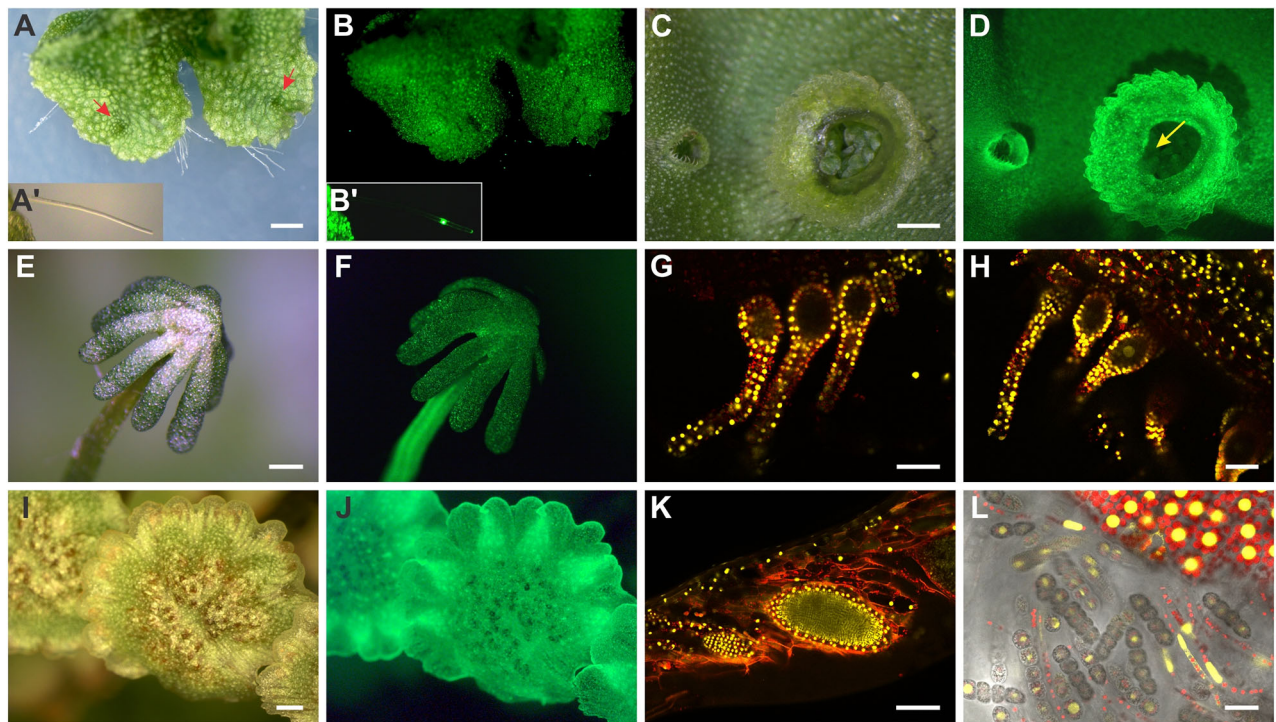
Taken together, MpFER is expressed in most tissues during the vegetative stages of gametophyte development as well as in the antheridia and archegonia during sexual reproduction. Interestingly, the $_{pro}$MpFER promoter was not active in mature gemmae and the unfertilized, quiescent egg cell, although expression was initiated after dormancy and in the zygote. In concordance with the collectively ubiquitous expression of CrRLK1Ls in *A. thaliana*, the MpFER expression pattern reinforces the importance of this family for basic cellular functions in land plants.

MpFER controls cell expansion during vegetative gametophyte development

To analyze the function of MpFER, three independent artificial microRNA constructs targeting MpFER were designed (amiR-MpFER), based on the endogenous microRNA MpmiR160 (Fig. S2; Flores-Sandoval et al., 2016) and driven by the ubiquitous $_{pro}$MpEF1 promoter (Althoff et al., 2014). Whereas amiR-MpFER1 and amiR-MpFER2 target sites in the ECD coding sequence, amiR-MpFER3 targets the sequence encoding the kinase domain (Fig. 3A,B). For each amiR-MpFER construct, several independent transgenic lines were obtained that showed a reduction in thallus size (Fig. 3C,D, Fig. S3A). MpFER levels were quantified by quantitative reverse transcription PCR (qRT-PCR) in two independent amiR-MpFER2 and amiR-MpFER3 lines each, which showed a similar phenotype (Fig. 3E). MpFER expression ranged from 10% to 20% of the wild-type level in all amiR-MpFER lines analyzed (Fig. 3E).

Previously, the T-DNA insertion mutant Mpfer-1 was identified in a screen for mutants with defective rhizoids (Honkanen et al., 2016; referred to as Mpthe). As the T-DNA inserted into the 3′ UTR of the MpFER gene (Fig. 3A; Honkanen et al., 2016), MpFER expression was analyzed by qRT-PCR, but it showed no reduction compared with the wild type (Fig. S3B), suggesting that the T-DNA insertion does not affect MpFER transcription. Sequencing of the MpFER coding sequence in the Mpfer-1 mutant did not show any

Fig. 2. MpFER is broadly expressed in most tissues throughout the *M. polymorpha* life cycle. (A-L) Expression of $_{pro}$MpFER:trpVNS in different organs of male and female *M. polymorpha* plants. Fluorescence is visualized as either green (epifluorescence microscope) or yellow (confocal microscope), depending on the panel. (A-F) Brightfield (A,C,E) and epifluorescence (B,D,F) images of a thallus (A,B), rhizoid (A′,B′), gemmae cups (C,D) and an archegoniophore (E,F). Red arrows indicate meristematic zones, the yellow arrow a gemma. Scale bars: 0.5 mm. (G,H) Confocal images of archegonia before (G) and 2 days after (H) fertilization. Scale bar: 50 µm. (I,J) Brightfield (I) and epifluorescence (J) images of an antheridiophore. Scale bar: 1 mm. (K) Confocal image of antheridia. Scale bar: 100 µm. (L) Confocal image of sporophyte and spores. Scale bar: 25 µm.
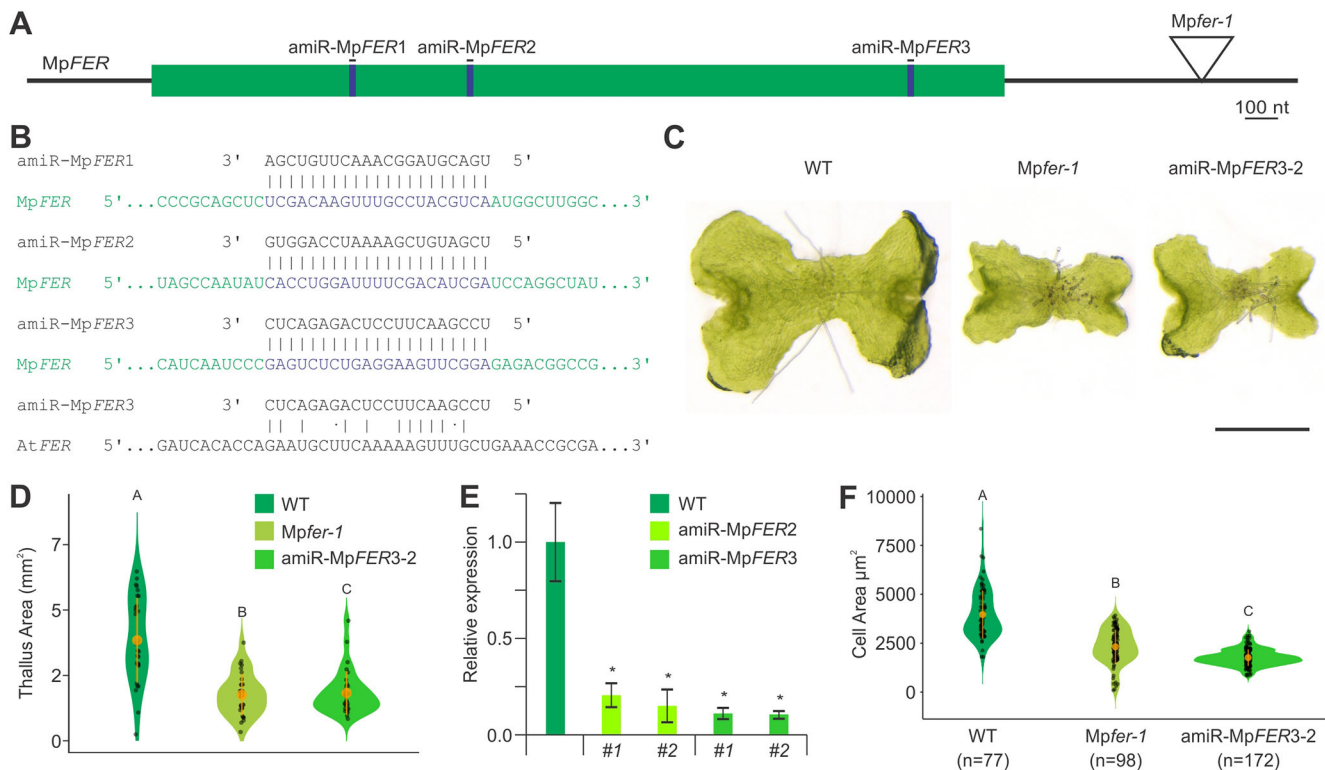
DEVELOPMENT

Fig. 3. Mp*FER* controls cell size during gametophyte development. (A) Representation of the mature Mp*FER* mRNA. The coding sequence is in green, locations of the amiRNA target sites in blue. The location of the T-DNA insertion in Mp*fer-1* is shown. (B) Base complementary of mature amiR-Mp*FER*1, amiR-Mp*FER*2 and amiR-Mp*FER*3 with the Mp*FER* transcript. Very low complementarity was found between amiR-Mp*FER3* and At*FER*. (C) Representative pictures of 10-day-old gemmalings of wild-type (WT), Mp*fer-1* and amiR-Mp*FER*3-2 lines. Scale bar: 1 mm. (D) Violin plot of thallus area of 14-day-old gemmalings of WT, Mp*fer-1* and amiR-Mp*FER*3-2 lines. $n=30$. Different letters indicate significant differences according to the non-parametric Kruskal–Wallis test and Dunn's test for multiple comparisons ($P<0.001$). Orange circles indicate the group mean and the corresponding vertical bars the standard deviation for each group. (E) Relative expression level of Mp*FER* in thallus tissue from WT and two independent insertion lines of amiR-Mp*FER*2 and amiR-Mp*FER*3, as measured by qRT-PCR. Mp*EF1* was used as internal control. Shown are mean±s.e.m. of three biological replicates. Statistical analysis was performed by one-way analysis of variance (ANOVA) followed by a post-hoc Duncan test (*$P<0.01$). (F) Violin plot of cell size in WT, *Mpfer-1* and amiR-Mp*FER*3-2 lines. Only areas with fully expanded cells in approximately 3-week-old plants were used for measurements. Different letters indicate significant differences according to the non-parametric Kruskal–Wallis test and Dunn's test for multiple comparisons ($P<0.001$). Orange circles indicate the group mean and the corresponding vertical bars the standard deviation for each group. See also Figs S2 and S3.

mutation, and 3′ RACE-PCR showed that transcript terminated about 1.3 kb inside the T-DNA and was not polyadenylated (Fig. S3C). Because the thallus size of Mp*fer-1* mutants is similar to that of amiR-Mp*FER* lines (Fig. 3C,D, Fig. S3A) and efficient translation depends on the presence of a poly(A)-tail (Sachs and Varani, 2000), we propose that MpFER protein levels are reduced in the Mp*fer-1* mutant despite normal transcript levels.

Rhizoids are tip-growing cells analogous to the root hairs of flowering plants (angiosperms). Reduced Mp*FER* activity strongly impaired rhizoid formation and the rhizoids collapsed (Fig. S3D). This had also been reported for the Mp*fer-1* mutant (Honkanen et al., 2016) and is in concordance with the function of At*FER* and At*ANX1/2* in tip-growing root hairs (Bai et al., 2014; Duan et al., 2010; Haruta et al., 2014; Gonneau et al., 2018) and pollen tubes (Boisson-Dernier et al., 2009; Miyazaki et al., 2009), respectively. As *Cr*RLK1L members are important for cell expansion in angiosperms (Hématy et al., 2007; Guo et al., 2009a; Kessler et al., 2010; Li et al., 2015; Dünser et al., 2019; Gachomo et al., 2014; Merz et al., 2017), the size of epidermal thallus cells in fully differentiated regions with minimal growth was measured in Mp*fer-1* and amiR-Mp*FER* lines, showing a reduction in cell area compared with the wild type (Fig. 3F, Fig. S3E,F). The average epidermal cell area was similarly reduced, although the distribution of cell areas differed between amiR-Mp*FER* lines and Mp*fer-1* (Fig. 3F, Fig. S3E,F).

In conclusion, Mp*FER* has a fundamental role in rhizoid formation and cellular growth during vegetative development. These results suggest an ancestral and conserved function of the *Cr*RLK1Ls in polar tip growth and cell expansion.

Mp*FER* is important for the morphological integrity of the gametophyte

Given that Mp*fer-1* and amiR-Mp*FER* lines retain some MpFER activity, we generated Mp*fer* knockout mutants with the goal of unveiling potentially hidden *Cr*RLK1L functions by generating a plant without any *Cr*RLK1L activity. Using CRISPR/Cas9, two sites in the ECD-coding sequence of Mp*FER* were targeted (Fig. 4A,B). At least ten independent lines were selected and analyzed for each target site. All plants with severely affected thallus development contained a frame-shift mutation at the respective target site (Fig. 4B,C) but Mp*FER* was not affected in transgenic plants with normal development.

The thallus area of the newly generated, amorphic knockout mutants was more strongly reduced compared with Mp*fer-1* (Honkanen et al., 2016), confirming that, like the amiR-Mp*FER* lines, Mp*fer-1* is a hypomorphic mutant (Fig. 4C,D). In contrast, rhizoid integrity was similarly affected in hypo- and amorphic Mp*fer* alleles, suggesting that rhizoid formation is more sensitive to reduced Mp*FER* activity than is thallus growth (Fig. 4E,F). Despite
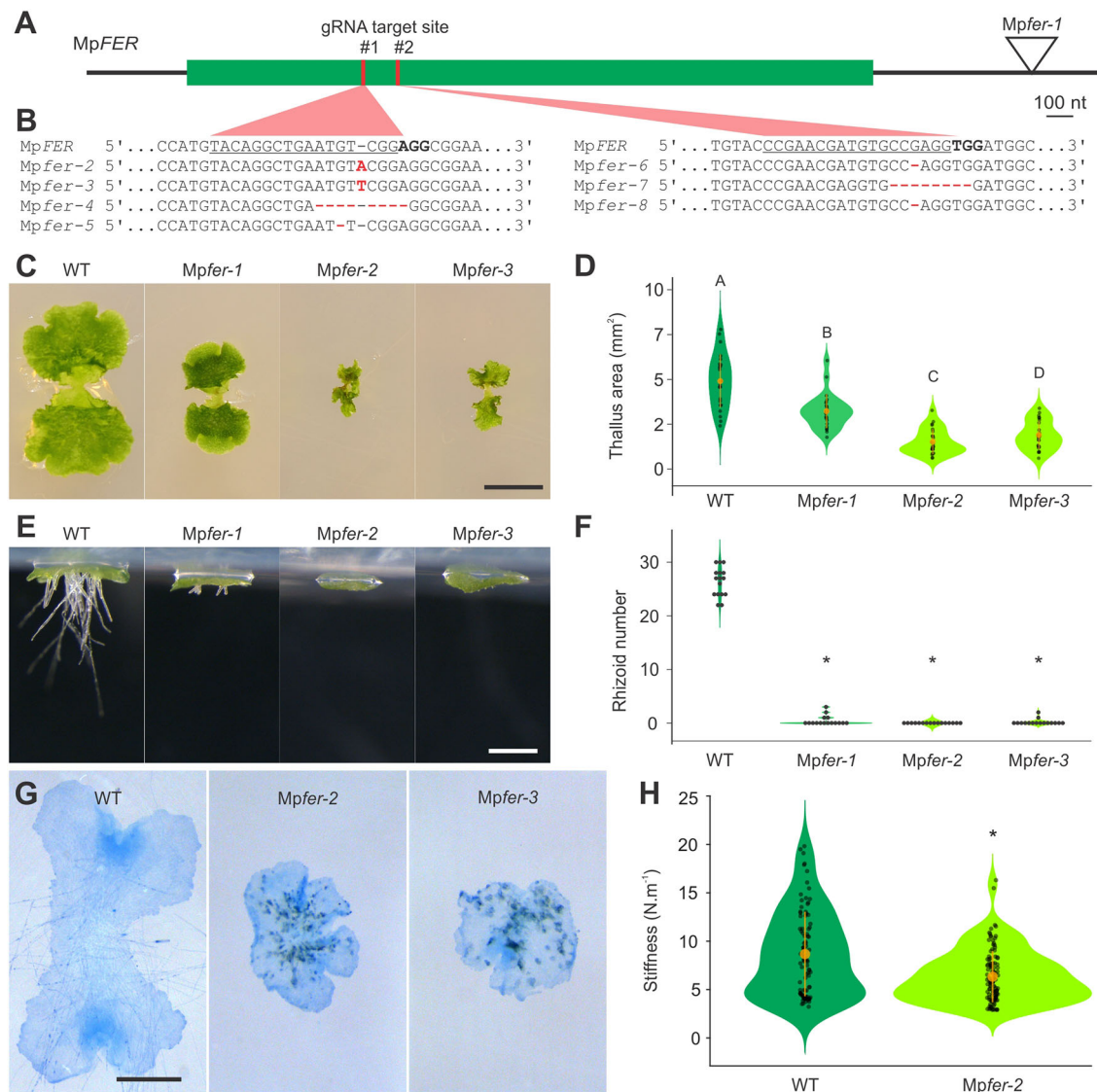
Fig. 4. The integrity of thalli from Mp*fer* knockout lines is severely affected. (A) Representation of the mature Mp*FER* mRNA with the coding sequence in green, and the location of the gRNA target sites in red. (B) Sequences of gRNA target sites in the confirmed Mp*fer* knockout mutants. Deletions and insertions are highlighted in red. (C) Representative pictures of 14-day-old gemmalings of the wild type (WT), Mp*fer-1* and two independent Mp*fer* knockout mutants. Scale bar: 0.5 cm. (D) Violin plot of thallus area of 7-day-old gemmalings of WT, Mp*fer-1* and two independent Mp*fer* knockout mutants. $n=25$. Different letters indicate significant differences in a one-way analysis of variance (ANOVA) followed by a post-hoc Duncan test ($P<0.01$). Orange circles indicate the group mean and the corresponding vertical bars the standard deviation for each group. (E) Representative pictures of 7-day-old gemmalings growing in upside-down plates of WT, Mp*fer-1* and two independent Mp*fer* knock-out mutants. Scale bar: 500 µm. (F) Violin plot of rhizoid number in 3-day-old gemmalings of WT, Mp*fer-1* and two independent Mp*fer* knockout mutants. $n=16$. Statistical analysis was performed by one-way analysis of variance (ANOVA) followed by a post-hoc Duncan test (*$P<0.01$). (G) Trypan Blue staining of 7-day-old gemmalings of WT, Mp*fer-1* and two independent Mp*fer* knockout mutants. Scale bar: 1 mm. (H) Violin plot of the reduction in the apparent stiffness of gemmaling tissue in Mp*fer-2* compared with the WT. Statistical analysis was performed using a Kruskal–Wallis test followed by a Tukey-Kramer post-hoc test (*$P<0.001$). Orange circles indicate the group mean and the corresponding vertical bars the standard deviation for each group.

the strong impact on thallus development, both hypo- and amorphic Mp*fer* mutants form gemma cups.

The strong disruption of thallus growth in amorphic Mp*fer* mutants prompted us to investigate whether cells of the thallus died in the absence of Mp*FER* activity. Indeed, using Tryphan Blue staining, we detected dead cells in these mutants, indicating a loss of morphological integrity (Fig. 4G). To investigate the mechanical properties of thallus cells, we measured their apparent stiffness using cellular force microscopy on 3-day-old gemmalings (plantlets derived from a gemma) and found that amorphic Mp*fer-2* mutants had a lower apparent stiffness than the wild type (Fig. 4H).

The apparent stiffness of the thalli depends on both the stiffness of the cell wall and the turgor pressure of the cells. Because the apparent stiffness is lower in Mp*fer-2* mutants, it is likely that a reduction in the stiffness of their cell wall causes the cells to burst and die.

Some reproductive but not all CWI-sensing functions of *Cr*RLK1Ls are conserved in land plants
In *A. thaliana*, at least seven *Cr*RLK1L family members play a role in reproduction, with At*ANX1/2* and At*BUPS1/2* being important for pollen tube growth (Boisson-Dernier et al., 2009; Miyazaki

et al., 2009; Zhu et al., 2018; Ge et al., 2017) and At*FER*, At*HERK1* and At*ANJ* for pollen tube reception by the synergid cells (Escobar-Restrepo et al., 2007; Galindo-Trigo et al., 2020). To characterize the function of Mp*FER* in reproductive development, amiR-Mp*FER3* lines were transferred to sexual organ-inducing conditions (Chiyoda et al., 2008). The number of antheridiophores

produced was significantly lower in amiR-Mp*FER* lines compared with the wild type (Fig. 5A, Fig. S3G) and the antheridiophore splash platforms were also smaller (Fig. 5B). The reduction in Mp*FER* expression in antheridiophores of amiR-Mp*FER* lines was confirmed by qRT-PCR and results were comparable to those using thallus tissue (Fig. 5C). A pronounced reduction in spermatogenous
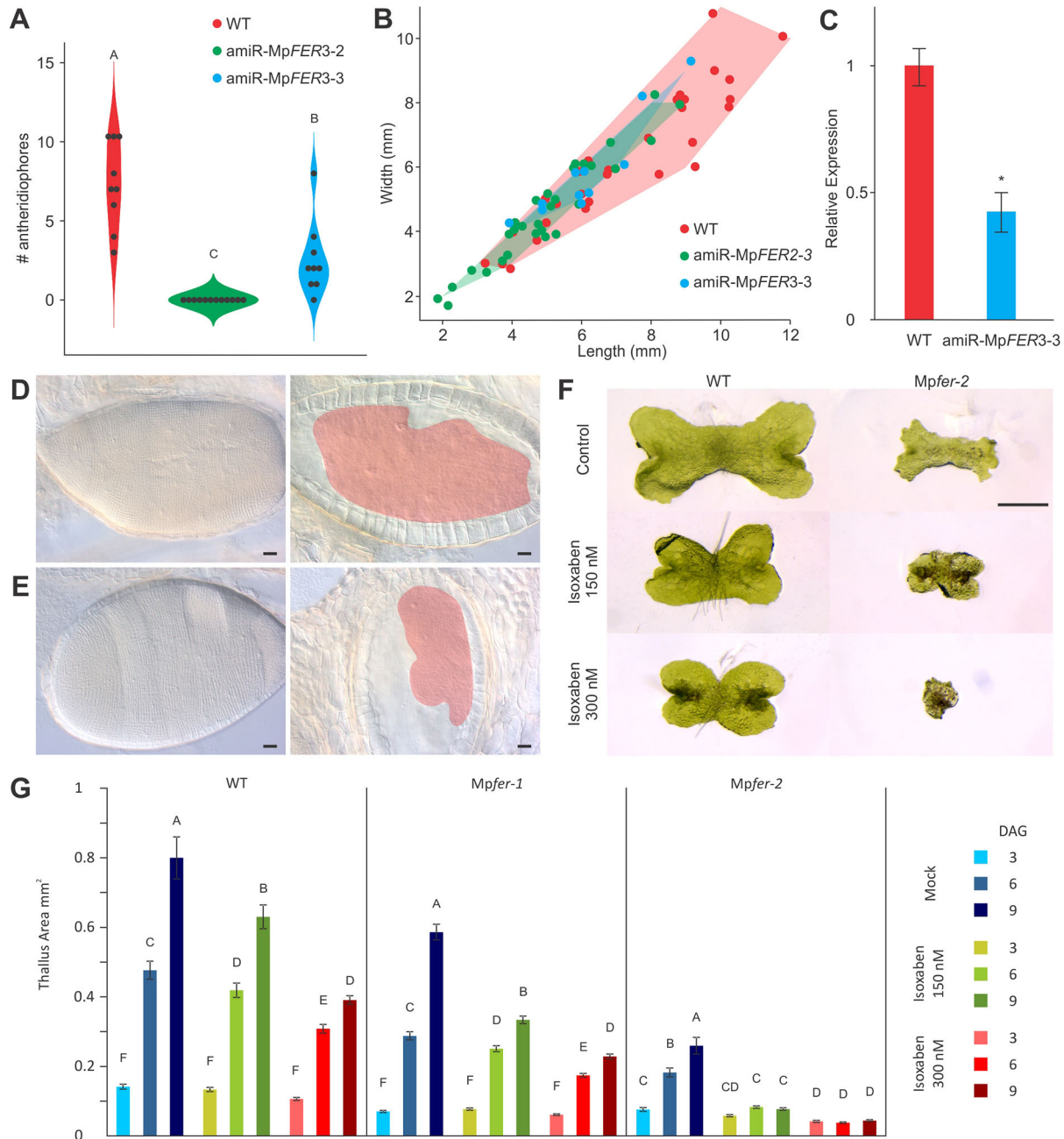
Fig. 5. Conservation of *Cr*RLK1L function in land plants. (A) Violin plot of the number of antheridiophores produced per plant for wild type (WT, *n*=9) and two independent amiR-Mp*FER*3 lines (amiR-Mp*FER*3-2, *n*=9; amiR-Mp*FER*3-3, *n*=12). Different letters indicate a significant difference in a one-way analysis of variance (ANOVA) followed by a post-hoc Duncan test (*P*<0.01). (B) Antheridiophore splash platform size distribution of WT (*n*=32), amiR-Mp*FER*2-3 (*n*=34) and amiR-Mp*FER*3-3 (*n*=11) lines. For all antheridia with a stalk >8 mm, length and width of the platform were recorded. Shaded areas represent the range of data points, illustrating the larger variation of splash platform size in the WT. (C) qRT-PCR of Mp*FER* levels in antheridiophores in a WT and amiR-Mp*FER*3-3 line. Mp*EF1* was used as internal control. Shown are mean±s.e.m. of three biological replicates. Statistical analysis was performed by one-way analysis of variance (ANOVA) followed by a post-hoc Duncan test (**P*<0.01). (D,E) Brightfield images (left) and optical cross-sections (right) of mature antheridia of a WT (D) and amiR-Mp*FER*3-3 line (E). The spermatogenous areas are shaded in red. Scale bars: 100 μm. (F) Representative pictures of 6-day-old gemmalings of WT and Mp*fer-2* mutants at different isoxaben concentrations. Scale bar: 1 mm. (G) Thallus area of gemmalings of WT, Mp*fer-1* and Mp*fer-2* lines growing on media containing different isoxaben concentrations. *n*=35. Data are mean±s.e.m. of two biological replicates. Different letters indicate a significant difference in a one-way analysis of variance (ANOVA) followed by a post-hoc Duncan test (*P*<0.05). DAG, days after gemmae-plating. See also Fig. S3.

tissue was observed in many antheridia isolated from amiR-MpFER3-3 lines (Fig. 5D,E). Whether this phenotype is caused by reduced cell expansion, as was observed in thalli, or by a lower cell division rate is currently unclear. Moreover, although the plants were grown under optimal conditions in axenic culture boxes, the effects on reproductive structures could be partly indirect and due to the reduction in plant size and/or rhizoid function.

To determine male fertility of these amiR-MpFER lines with reduced spermatogenous tissue, we performed crosses with wild-type female plants. The spermatocyte concentration harvested from wild-type antheridia was almost threefold higher than from amiR-MpFER lines and was adjusted using a hemocytometer. In just one of the crosses (n=20), a single sporophyte was formed, resulting in 0.05±0.05 (mean±s.e.m.) sporophytes per archegoniophore, whereas the same females crossed with wild-type males yielded 9.95±2.33 (mean±s.e.m.) sporophytes per archegoniophore. In summary, MpFER plays a role in antheridiophore development, and spermatocytes of plants with reduced MpFER activity are poorly fertile. Thus, CrRLK1Ls have a conserved role in reproduction in addition to their role in cell expansion and integrity during vegetative development.

Some A. thaliana CrRLK1Ls are involved in surveying CWI and in inhibiting growth when CWI is impaired. Cell wall defects caused either by mutations affecting cellulose biosynthesis or by treatment with isoxaben, a cellulose synthesis inhibitor, can be suppressed by a mutation in AtTHE1 (Hématy et al., 2007; Denness et al., 2011). To investigate whether MpFER also acts as CWI sensor, we treated wild-type, Mpfer-1 and Mpfer-2 gemmae with isoxaben (Fig. 5F,G). As in the wild type, isoxaben affected the development of gemmae with reduced MpFER activity, all growing progressively less with increasing isoxaben concentration (Fig. 5F,G). Moreover, isoxaben treatment was lethal for Mpfer-2 knockout mutants (Fig. 5F,G). Similar observations were reported for Atfer-4, where isoxaben treatment increased the number of dead cells in hypocotyls (Malivert et al., 2021). These results suggest that the function of AtTHE1 in repressing cellular growth when CWI is impaired appeared later in the course of land plant evolution or was lost in the Marchantia lineage.

The CrRLK1L signaling pathway is conserved in land plants
As downregulation of MpFER or AtFER produce similar phenotypes concerning polarized growth and cell expansion in M. polymorpha and A. thaliana, respectively, interspecific complementation was attempted. First, the coding sequence of MpFER fused to the Green Fluorescent Protein (GFP) gene under the control of the viral 35S promoter ($_{pro}$35S:MpFER-GFP) was transformed into heterozygous Atfer-1 mutants. Then, GFP expression at the cell periphery and complementation of the bursting root hair and reduced rosette size phenotypes were assessed in transgenic plants (Fig. 6A). Atfer-1 homozygotes expressing the MpFER-GFP protein look similar to Atfer-1 mutants, indicating that MpFER does not complement these Atfer-1 loss-of-function phenotypes (Fig. 6A). Although we cannot exclude the possibility that this is because we used a heterologous promoter, we consider this unlikely as expression the 35S promoter is routinely used to complement root hair phenotypes (Baumberger et al., 2001; Kim and Dolan, 2016). In a complementary experiment, the coding sequence of AtFER fused to the Citrine gene under the control of the MpEF1 promoter ($_{pro}$MpEF1:AtFER-Cit) was transformed into amiR-MpFER3-2 plants. Ten independent lines with Citrine expression at the cell periphery were phenotypically characterized (Fig. 6B,C). All had bursting rhizoids and a reduced thallus size,

similar to the parental amiR-MpFER3-2 line, suggesting that AtFER does not rescue the vegetative phenotypes produced by downregulation of MpFER. A sequence alignment of AtFER with amiR-MpFER3 showed no complementarity (Fig. 3B), confirming that the failure to complement is not caused by a potential downregulation of AtFER by amiR-MpFER3. Taken together, these results show that MpFER and AtFER cannot substitute for each other with respect to their function in cell expansion and tip growth.

In A. thaliana, it was shown that AtFER forms a complex with AtRALF peptides and the LRE/LLG co-receptors (Xiao et al., 2019). As no interspecific complementation was observed, the conservation of binding surfaces between CrRLK1L, RALF and LRE homologs were analyzed. The M. polymorpha genome encodes three RALF peptides [MpRALF: Mp1g27120 (Mapoly0002s0166); MpRALF2: Mp2g21670 (Mapoly0040s0047); MpRALF3: Mp7g07270 (Mapoly0076s0067)] (Galindo-Trigo et al., 2016; Bowman et al., 2017). We performed phylogenetic analysis using the amino acid sequences of the predicted mature peptides of A. thaliana and M. polymorpha RALFs (Fig. S4A). All MpRALF peptides clustered together with AtRALFs known to interact with CrRLK1L receptors, including AtRALF1 and AtRALF23, which serve as AtFER ligands (Stegmann et al., 2017; Haruta et al., 2014) (Fig. S4A). The MpRALFs shared the four conserved Cys residues as well as the YXXY and YY motifs with the AtRALF1 subgroup (Fig. S4B). However, only MpRALF1 and MpRALF3 had an RRXL motif, which is important for cleavage by the S1P protease (Fig. S4B,C) (Srivastava et al., 2009), consistent with the presence of one S1P ortholog in basal plants [Mp8g07990 (Mapoly0155s0018); Fig. S4D]. There are two MpLRE/LLG proteins encoded in the M. polymorpha genome (Fig. S5A,B). Both the MpLRE1 [Mp5g09600 (Mapoly0048s0110)] and MpLRE2 [Mp4g22100 (Mapoly0090s0020)] proteins showed conservation of the eight Cys residues and the ND motif characteristic of the family (Fig. S5B); however, MpLRE1 did not contain a GPI-anchoring site (Fig. S5B). Structure prediction using AtLLG1 as a template (Xiao et al., 2019) showed a conserved general structure (Fig. S5C,D). Some of the MpRALF and MpLRE family members showed a similar expression pattern as MpFER (Fig. S5F), suggesting that the corresponding proteins could form a complex similar to that described in A. thaliana.

To gain insights into the formation of a putative CrRLK1L signaling complex, the MpFER/MpRALF/MpLRE complex was modeled. The general structure appeared to be conserved (Fig. S5E); however, analysis of conserved sites between M. polymorpha and A. thaliana showed a low amino acid conservation in the interacting surfaces of the complex subunits (Fig. 6D). This suggests that the lack of interspecific complementation may be due to differences in amino acids that are important for complex formation, and that the proteins forming the complex have diverged, following distinct routes of co-evolution in the two lineages.

Because interspecific complementation of the amiR-MpFER phenotypes was unsuccessful, we investigated whether suppression using a downstream component of CrRLK1L signaling identified in A. thaliana was possible. AtMRI, a receptor-like cytoplasmic kinase, acts downstream of AtFER or AtANX1/2 in the regulation of polar tip growth (Boisson-Dernier et al., 2015; Liao et al., 2016). The dominant AtMRI^{R240C} mutation can suppress pollen tube rupture in the Atanx1 Atanx2 double mutant and the root hair defects of Atfer-4 (Boisson-Dernier et al., 2015; Liao et al., 2016). A mutation in MpMRI (also known as MpPTI), with a bursting rhizoid phenotype similar to that observed in Mpfer-1, was

8
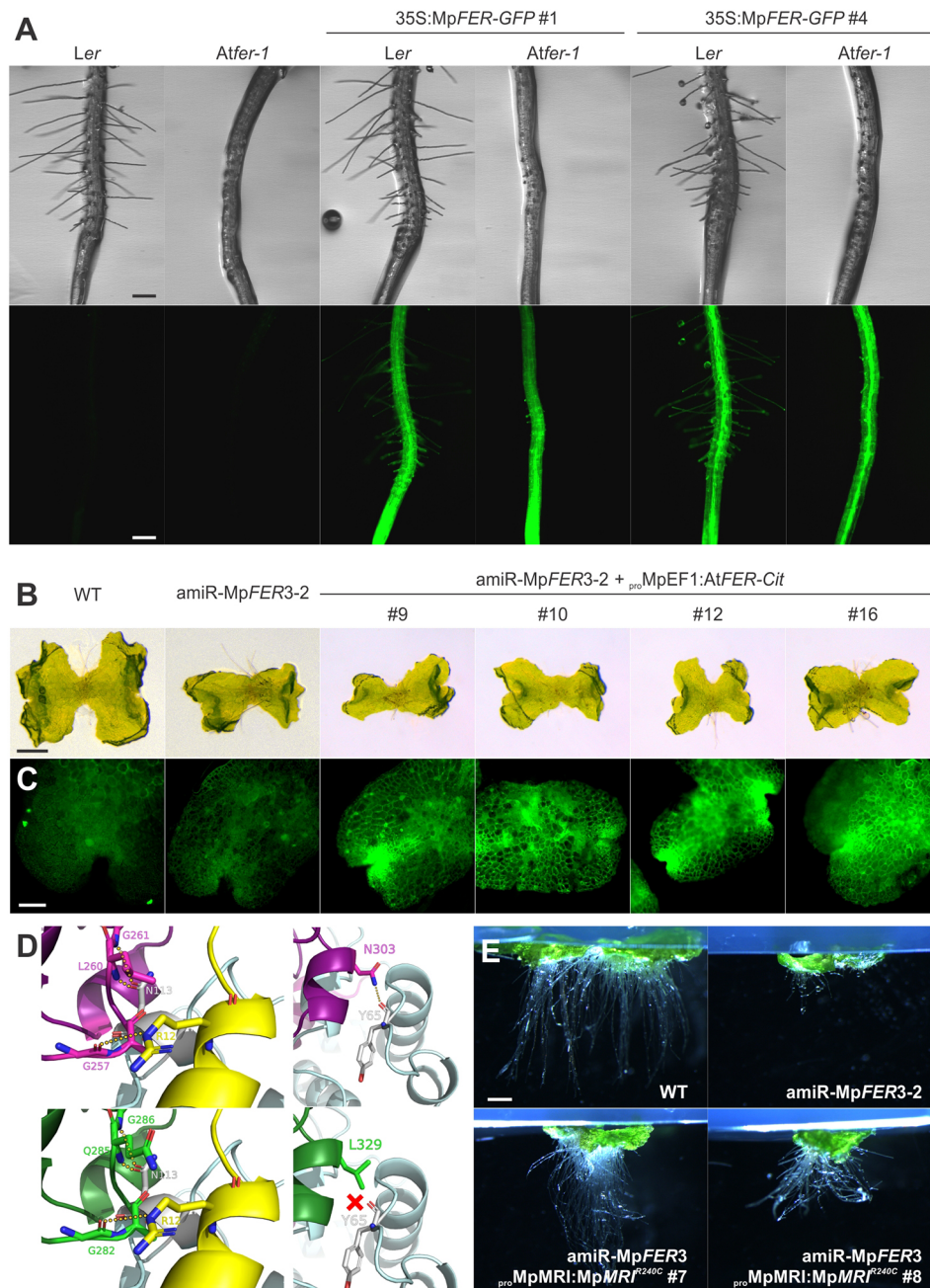
Fig. 6. Interspecific complementation of *A. thaliana* and *M. polymorpha* plants with reduced levels of *FER* activity. (A) Bright-field (upper row) and epifluorescence (lower row) pictures of roots of independent *A. thaliana* lines expressing $_{pro}$*35S:*Mp*FER-GFP* in L*er* wild-type (WT) and At*fer-1* plants. Scale bars: 200 μm. (B) Ten-day-old gemmalings of WT and amiR-Mp*FER*3-2 *M. polymorpha* plants with and without expression of At*FER-Cit*. Scale bar: 0.5 mm. (C) Citrine expression in 7-day-old gemmalings of WT and amiR-Mp*FER*3-2 plants with and without expression of At*FER-Cit*. Scale bar: 100 μm. (D) Schematics of the *Cr*RLK1L^{ECD} polar interactions sites with LRE/RALF when forming a protein complex. Upper panels correspond to contact areas between AtFER (purple), AtLLG2 (blue-gray) and AtRALF23 (yellow), and lower panels to the modeled MpFER structure (green) superimposed onto the same complex. Polar interactions are depicted as dotted yellow lines. Left panels show the predicted polar interactions of the complex that are conserved between *A. thaliana* and *M. polymorpha*, whereas the right panels show the polar interaction between AtFER and AtLLG2 that is predicted to be absent between MpFER and AtLLG2. (E) Suppression of the amiR-Mp*FER* phenotype by a dominant-active version of Mp*MRI* under its own promoter ($_{pro}$Mp*MRI*:Mp*MRI^{R240C}*). In addition to the WT and amiR-Mp*FER*3-2 controls, two independent $_{pro}$Mp*MRI*:Mp*MRI^{R240C}* lines with partial suppression of the rhizoid phenotype are shown. Scale bar: 1 mm. See also Figs S4-S6.

identified in the same genetic screen for *M. polymorpha* mutants with defective rhizoids (Honkanen et al., 2016). To test whether Mp*MRI* is a conserved downstream component of the Mp*FER* signal transduction pathway, a dominant-active form of the protein equivalent to AtMRI^{R240C} was transformed into the amiR-Mp*FER*3-2 line, driven by 2 kb of the endogenous promoter ($_{pro}$Mp*MRI*:Mp*MRI^{R240C}*). Several independent lines showed a partial restoration of rhizoid growth; however, we also observed defects in thallus development of lines with higher levels of Mp*MRI* expression, mainly abnormalities in the epidermis (Fig. 6E, Fig. S6A-E). This suggests that Mp*MRI* acts downstream of Mp*FER* in the signal transduction pathway controlling polarized growth since the origin of land plants, in agreement with a recent report on the functional characterization of Mp*MRI* (Westermann et al., 2019).

Overexpression of Mp*FER* affects morphological integrity

Because overexpressing At*FER* in *M. polymorpha* did not lead to any obvious phenotypes or complementation of amiR-Mp*FER* lines (Fig. 6B,C), we also overexpressed At*FER* and Mp*FER* in the wild type. As in the amiR-Mp*FER* background, overexpression of AtFER ($_{pro}$Mp*EF1:*At*FER-Cit*) in a wild-type background had no effect, consistent with the idea that At*FER* is unable to form a complex with the corresponding *M. polymorpha* proteins. However, when expressing an MpFER-Citrine fusion protein ($_{pro}$Mp*EF1:* Mp*FER-Cit*) in wild-type plants, thallus development was strongly affected (Fig. 7A). As expected, MpFER-Cit localized to the membrane (Fig. 7A, inset), and higher protein levels correlated with a more severe phenotype (Fig. S6F,G). Scanning electron microscopy of the epidermis of plants expressing high levels of Mp*FER* showed defects in the formation of air chambers and air
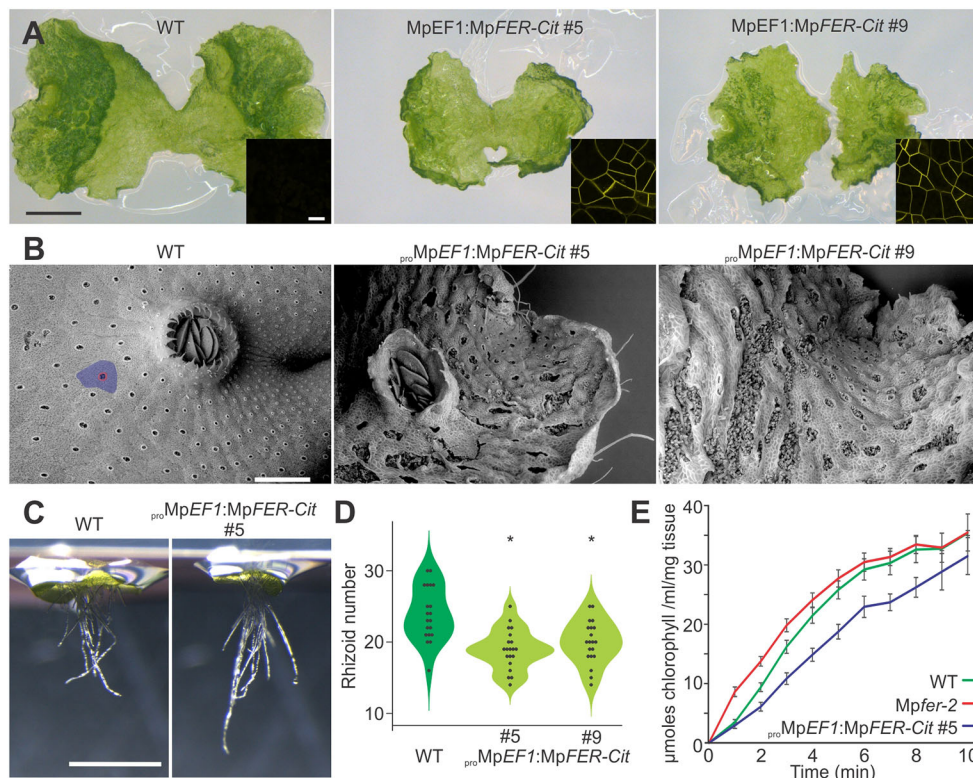
Fig. 7. Overexpression of Mp*FER* affects morphological integrity.
(A) Representative pictures of 10-day-old gemmalings of wild type (WT) and two different lines overexpressing Mp*FER* (_pro_Mp*EF1*:Mp*FER-Cit*). Scale bar: 1 mm. Insets show Citrine expression at the plasma membrane in _pro_Mp*EF1*:Mp*FER-Cit* lines #5 and #9 as observed by confocal microscopy. Scale bar: 20 μm. (B) Scanning electron microscopical images of thalli from 20-day-old plants of WT and _pro_Mp*EF1*:Mp*FER-Cit* lines #5 and #9. The blue region demarks an air chamber, and air pore cells are colored in red. Scale bar: 500 μm. (C) Representative pictures of 3-day-old gemmalings growing in upside-down plates of WT and _pro_Mp*EF1*:Mp*FER-Cit* #5 lines. Scale bar: 1 mm. (D) Violin plot of the number of rhizoids in 3-day-old gemmalings of WT and _pro_Mp*EF1*:Mp*FER-Cit* lines #5 and #9. *n*=20. Statistical analysis was performed by one-way analysis of variance (ANOVA) followed by a post-hoc Duncan test (**P*<0.01). (E) Graphs showing the amount of effluxed chlorophyll as a function of time from 15-day-old gemmalings of WT, Mp*fer-2* and _pro_Mp*EF1*:Mp*FER-Cit* #5 lines. See also Fig. S6.

pores (Fig. 7B), similar to what we observed when expressing the dominant-active Mp*MRI^R240C* (Fig. S6A-C). This phenotype is reminiscent of the *quasimodo1* mutant in *A. thaliana*, in which cell walls have a reduced pectin content and cell adhesion is compromised (Bouton et al., 2002). Moreover, overexpression of Mp*FER* affects the number of lobes in the antheridial receptacle, producing only four instead of eight lobes (Fig. S6H), supporting the importance of Mp*FER* for sexual development. Considering the importance of Mp*FER* for normal rhizoid formation, we also analyzed rhizoids in the _pro_Mp*EF1*:Mp*FER-Cit* lines: although rhizoid morphology looked normal, a decrease in rhizoid number was observed (Fig. 7C,D). To analyze cell wall properties of Mp*FER* overexpressor lines, chlorophyll efflux rates were measured as an indicator of epidermal permeability (Fig. 7E). Overexpression of *MpFER* clearly reduced the chlorophyll efflux compared with the wild type, whereas the opposite was observed in Mp*fer-2* mutants (Fig. 7E). Taken together, the results obtained by overexpressing Mp*FER* support a role of Mp*FER* in cell wall formation and the maintenance of tissue integrity during plant morphogenesis.

DISCUSSION

During land plant evolution, many developmental aspects have changed in order to adapt to new environments, producing the enormous diversity observed in the plant kingdom. However, the control and maintenance of CWI remained a key aspect for the biology of a plant cell. CWI sensing is not only important for vegetative growth by cell expansion, but it is also essential for sexual reproduction and defense responses.

The *Cr*RLK1L family was first characterized for its importance during angiosperm fertilization, a process comprising aspects of polar cell elongation, CWI control, and cell-cell communication (Escobar-Restrepo et al., 2007; Huck et al., 2003; Rotman et al., 2003). Lately, different members of this family were found to carry

out diametrically opposite roles in diverse aspects of plant development, which has made it difficult to define the core or ancestral function of this gene family comprising 17-members in *A. thaliana* (Escobar-Restrepo et al., 2007; Hématy et al., 2007; Boisson-Dernier et al., 2009; Guo et al., 2009a,b; Kessler et al., 2010; Bai et al., 2014; Miyazaki et al., 2009; Keinath et al., 2010; Duan et al., 2010; Galindo-Trigo et al., 2020; Zhu et al., 2018; Li et al., 2015; Richter et al., 2017; Ge et al., 2017).

Here, we report the characterization of the single *Cr*RLK1L gene encoded in the genome of *M. polymorpha*. Structurally, the MpFER ECD and kinase domain share similarities with previously characterized *Cr*RLK1L members, including the malectin-like domain and conserved phosphorylation sites. Conservation of RALF and LRE members in *M. polymorpha* suggests that MpFER also forms a complex at the plasma membrane (Xiao et al., 2019). Although modeling predicted that the general structure of the complex was conserved, the interaction surfaces seem to have diverged and co-evolved independently in the respective lineages.

We observed a broad involvement of MpFER at both vegetative and reproductive stages of development. During vegetative growth of the gametophyte, Mp*FER* is required for rhizoid formation and cell expansion, but it also plays a role in male gametogenesis and is expressed in female reproductive organs. These findings suggest that the *Cr*RLK1Ls have, also in ancestral land plants, held roles in various aspects of both vegetative and reproductive development. Thus, the role of *Cr*RLK1Ls in angiosperm reproduction does not represent a derived feature from a purely vegetative function in cell elongation in bryophytes but constitutes a conserved feature of this gene family.

Moreover, the almost ubiquitous expression of Mp*FER* in *M. polymorpha* is consistent with the collective expression of different *Cr*RLK1L members in essentially all tissues and organs of *A. thaliana* (Lindner et al., 2012). Thus, gene duplication allowed

the expansion of the *Cr*RLK1L family in angiosperms, diversifying their expression patterns and functions but also leading to genetic redundancy (Boisson-Dernier et al., 2009; Galindo-Trigo et al., 2020; Ge et al., 2017; Lindner et al., 2012).

*Cr*RLK1L members are important sensors of CWI during polarized growth, both in pollen tubes (Boisson-Dernier et al., 2009; Ge et al., 2017) and root hairs (Duan et al., 2010). In early divergent land plants, rhizoids are tip-growing cells with a function analogous to that of root hairs, important for taking up nutrients and water (Honkanen et al., 2016; Bowen, 1935). Based on the conservation of many genes controlling the development and growth of tip-growing cells forming rooting systems, it was suggested that these pathways were active in the earliest land plants that existed about 470 million years ago (Honkanen et al., 2016). That Mp*FER* also controls rhizoid integrity points to the importance of the *Cr*RLK1L pathway for polarized growth since the origin of land plants. Moreover, the fact that amorphic Mp*fer* mutants contain many dead cells demonstrates the importance of the *Cr*RLK1L pathway for cellular integrity during vegetative growth. As the occurrence of dead cells was recently also reported in At*fer-4* mutant seedlings (Malivert et al., 2021), the function of this pathway in maintaining cellular integrity may also be ancestral. Whether Mp*FER* also plays a central role in plant innate immunity, as it does in angiosperms (Keinath et al., 2010; Stegmann et al., 2017), remains to be determined.

The signaling mechanisms downstream of Mp*FER* in *M. polymorpha* development are still unclear. Mutations affecting Mp*MRI*, the *M. polymorpha* ortholog of At*MRI* that acts downstream of AtFER and AtANX1/2 in *A. thaliana* during polarized growth (Boisson-Dernier et al., 2015), lead to a rhizoid phenotype similar to that of Mp*fer* (Honkanen et al., 2016; Westermann et al., 2019). The suppression of the rhizoid phenotype in amiR-Mp*FER* transformants with the constitutively active form MpMRI^{R240C} corroborates a conserved *Cr*RLK1L signaling cascade during polarized growth in *M. polymorpha*. However, whether this pathway also relies on Ca^{2+} and reactive oxygen species as second messengers, as it does in *A. thaliana*, remains to be determined.

In *A. thaliana*, loss-of-function mutations in the motor protein AtKINESIN-13a, a microtubule-based motor, cause cell elongation in petals, leaves and hypocotyls concomitant with changes in cell wall composition in leaves (Fujikura et al., 2014). This effect depends on functional At*THE1* and does not occur in At*kinesin-13a* At*the1* double mutants. Interestingly, in this case, At*THE1* stimulates cell elongation in response to defects in cell wall deposition (Fujikura et al., 2014). Based on our results, we have no indication that Mp*FER* acts as a CWI sensor and regulates growth similar to At*THE1* in response to cell wall disturbances. We have not observed a context in *M. polymorpha* development, in which Mp*FER* inhibits cell expansion. Therefore, the ability to restrict growth in response to disturbances in CWI could represent an evolutionarily derived feature, as gene duplication allowed for the diversification and specialization of *Cr*RLK1Ls to regulate cellular growth in a more complex and context-dependent way. The capacity to regulate growth flexibly appears to be fundamentally context dependent, as a similar discrepancy in promoting or inhibiting growth is also known for some well-studied growth-promoting agents, such as the phytohormones auxin and brassinosteroid, which can have growth-inhibitory effects dependent on tissue and concentration. The reverse was noted for the phytohormones ethylene and abscisic acid, which are usually considered growth inhibitors but can also promote growth, depending on the context (Pierik et al., 2006; Wolf and Höfte, 2014; Humplík et al., 2017).

Taken together, our results suggest an ancestral and conserved function of the *Cr*RLK1Ls in polar cell growth and cell expansion, but also during sexual reproduction. In addition, we probed the relevance of *Cr*RLK1L members for cell integrity and morphogenesis. In angiosperms, *Cr*RLK1Ls occupy an important position at the interface of developmental and environmental inputs, which are integrated by a downstream signaling machinery that controls cell shape and polar growth to ensure normal development, e.g. by preventing cell rupture upon CWI defects. Whether the same downstream machinery is utilized in a similar fashion in *M. polymorpha* remains to be shown, even though the similarity in function points to a related mechanism. Even less is known about upstream aspects of *Cr*RLK1L signaling. Future studies on the transcriptional regulation and the upstream components, such as the putative RALF ligand(s), in the highly simplified *M. polymorpha* system could provide fundamental insights into the molecular mechanism of the *Cr*RLK1L pathway, which is so central to land plant physiology, growth and development.

MATERIALS AND METHODS
Experimental model
M. polymorpha subsp. *ruderalis* (Bischl. & Boissel.-Dub.) plants of the Tak-1 or Tak-2 accession were grown on sterile culture on half-strength Gamborg's B5 basal medium (PhytoTech Labs), supplemented with 1% phytoagar in Petri dishes sealed with air-permeable tape. The plants were kept under fluorescent light and long-day conditions (16 h light at 22°C, 8 h dark at 20°C) in Percival growth cabinets (models AR-41L3 and AR-41/L2). Alternatively, to induce sexual reproduction, plants were cultivated in Jiffy pots filled with a 1:1 mixture of soil ('Einheitserde D73+Bims', Universalerde) and sand or in culture boxes (Duchefa Eco2 Box, E1654) in sterile culture on half-strength Gamborg's B5 basal medium, under fluorescent light supplemented with far-red light (GreenPower LED module HF far-red, 929000464503 and 929000632103 Philips).

For *Arabidopsis thaliana* L. (Heyn), wild-type plants in all experiments were of the L*er*-0 accession. The At*fer-2* mutant was obtained from the Signal Collection at the Salk Institute. Plants were grown in soil (ED73; Universalerde), covered with a thin quartz sand layer, under long photoperiods (16 h light/8 h dark) at 23°C and 60% relative humidity.

Phylogenetic analysis
Protein sequences were identified in plant genomes via BLASTp searches in https://phytozome.jgi.doe.gov/pz/portal.html. To elucidate the evolutionary relationship across land plant evolutionary history, we focused on *A. thaliana*, *Amborella trichopoda*, *Selaginella moellendorffii*, *Physcomitrium patens*, *Spagnum fallax*, *Ceratodon purpureus*, *Antoceros agrestis*, *A. punctatus* and *M. polymorpha* as representative species for angiosperms, lycophytes, mosses, hornworts and liverworts, respectively. Complete or partial coding protein sequences were aligned using ClustalW parameters and were conducted in MEGA7. Phylogenetic trees were constructed with the 'neighbor-joining' method, with a bootstrap test of 1000 replicates. The evolutionary distances were computed using the Poisson correction method.

Vector construction
Expression constructs
A BJ36 plasmid (Flores-Sandoval et al., 2015) containing a tripleVENUS-NLS (trpVNS) fragment was modified by adding a ligation-independent cloning (LiC) adapter site (De Rybel et al., 2011). A promoter fragment of Mp*FER* of 3.2 kb was amplified by PCR using the primers listed in Table S2 and cloned into the BJ36 vector via LiC cloning. The $_{pro}$Mp*FER* promoter fragment fused to trpVNS was then shuttled via NotI restriction sites into the HART01 (Flores-Sandoval et al., 2015) expression vector. The expression vector was also directly modified to contain the LiC sites, so promoter fragments could be directly cloned in front of trpVNS in the HART01 vector via LiC cloning. This vector was called VHL (trpVNS-containing HART01 vector with LiC sites).

DEVELOPMENT

11

amiRNA constructs

For functional analyses, three independent artificial microRNA (amiRNA) constructs were made (Fig. S2). The endogenous microRNA precursor Mp*miR160* was used as both backbone and template to design the constructs, which generated single species small RNA molecules of 21 nt length, complementary to the target gene transcript (Flores-Sandoval et al., 2016; Rövekamp et al., 2016). Three miR160 backbones containing independent amiR-Mp*FER*/amiR-Mp*FER** duplexes were synthesized by GenScript and fused to the $_{pro}$Mp*EF1* promoter in the BJ36 shuttle vector and shuttled to the HART01 expression vector as described previously (Rövekamp et al., 2016). The folding structure and design procedures have been explained in detail previously (Flores-Sandoval et al., 2016; Rövekamp et al., 2016). The sequences for the amiRNAs were designed to retain the exact physical properties of the endogenous Mp*miR160* template. The folding patterns were analyzed in Mfold software (Zuker, 2003) and the sequences synthesized (Fig. S2).

CRISPR/Cas gRNA

Selection of target sites was performed using CasFinder (Aach et al., 2014 preprint). Complementary oligos were designed and annealed for ligation into gRNA, in the pMpGE_En03 vector, previously digested with the BsaI restriction enzyme. Resulting gRNAs were incorporated into binary vector pMpGE011 through Gateway recombination.

Overexpression of Mp*FER* and At*FER*

The full-length Mp*FER* sequence was amplified from genomic *M. polymorpha* DNA with attB sites and Gateway-cloned via pDONR207. For *A. thaliana* expression, Mp*FER* was introduced into the expression vector pMDC201, which contains a *2X35S* promoter fragment and an in-frame C-terminal mGFP6 (Curtis and Grossniklaus, 2003). For *M. polymorpha* expression, Mp*FER* was introduced intro the binary vector pMpGWB308, which contains the $_{pro}$MP*EF1* promoter and an in-frame C-terminal Citrine (Ishizaki et al., 2015). Similarly, for expression of At*FER* in *M. polymorpha*, the coding sequence of At*FER* was introduced into the pMpGWB308 binary vector for the generation of the $_{pro}$Mp*EF1:*At*FER-Cit* construct.

qRT-PCR and droplet digital PCR (ddPCR)

RNA extraction from *M. polymorpha*

RNA extraction from thallus tissue (~100 mg including apical notch) was carried out using the RNeasy Plant Mini Kit (74904, QIAGEN). To remove contaminating DNA, the TURBO DNA-free Kit (AM1907, Ambion) was used according to the manufacturer's recommendations. To extract RNA from the gametophores (two antheridiophores of >5 mm diameter were pooled, respectively, for each replicate), the Direct(-zol) RNA MiniPrep (R2050, ZymoResearch) was used with the TRIzol Reagent (15596026, Ambion) according to the manufacturer's protocol, including on-column DNase digestion and subsequent TURBO DNA-free Kit treatment. RNA samples were quantified using the Qubit RNA HS Assay Kit (Q32852, Life Technologies), a Nanodrop ND-1000 Spectrometer or an Agilent 2100 BioAnalyzer.

cDNA synthesis

cDNA was synthesized from 0.5 μg or 1.0 μg of total RNA. Reverse transcription was performed in 25 μl with 20 μg/ml Oligo(dT) 12-18 primers and 200 units of SuperScript II Reverse Transcriptase (18064-014, Invitrogen) according to the manufacturer's protocol. The resulting cDNA was diluted 1:9 by adding nuclease-free water. To control for genomic DNA contamination, control replicates of all samples were incubated without SuperScript II reverse transcriptase.

Primer tests and qRT-PCR

Primer efficiency and concentration tests were carried out for Mp*FER* and suitable reference genes as described previously (Rövekamp et al., 2016; Althoff et al., 2014). Amplification experiments were carried out using a 7500 Applied Biosystem Fast Real-Time PCR System. Reactions were performed in 20 μl volumes containing 10 μl 2× SYBR Green Master Mix (SsoAdvanced™ Universal SYBR Green Supermix), 200 nM (Mp*EF1* and Mp*FER*) or 250 nM (Mp*ACTIN*) forward and reverse primers, and 1 μl diluted cDNA. Where possible, three technical and biological replicates were performed for each reaction. The primers used for qRT-PCR are summarized in Table S1.

ddPCR analysis

Individual PCR reactions were performed in a total volume of 25 μl, using 1× ddPCR EvaGreen Supermix, with droplets generated according to the manufacturer's recommendations. Reading of the PCR-amplified droplets was carried out using a QX200 Droplet Reader (Bio-Rad) and analyzed using QuantaSoft™ Software (v1.4, Bio-Rad). The counts from ddPCR were normalized through a log2 transformation. Afterwards, relative expression was calculated against the geometric mean of the counts for all three reference genes (Mp*ACT1*, Mp*ACT7* and Mp*APT3*) (Vandesompele et al., 2002): [log2(gene tested+1)−log2(geom. mean of all references+1)]. The primers used for the ddPCR are summarized in Table S1.

3′ RACE-PCR

RNA from wild-type and Mp*fer-1* mutant plants were extracted as previously described. A poly(G)-tail was added at the 3′ end of the RNA according to a Poly(A) Polymerase protocol (Thermo Scientific), using GTP instead of ATP. Reverse transcription was performed using anchored Oligo(dC) instead of Oligo(dT). Nested PCR on the cDNA was performed using two forward primers that matched the 3′ UTR sequence of Mp*FER* (3′RACE-Fwd1 and 3′ RACE-Fwd2) and Oligo(dC) that are listed in Table S1. PCR fragments were purified and sequenced.

Transformation of *M. polymorpha* and *A. thaliana*

Agrobacterium-mediated transformation using regenerating thalli of *M. polymorpha* was performed by co-cultivation of 15-day-old plant fragments with transformed *Agrobacterium tumefaciens* (GV3101) cells (Kubota et al., 2013; Ishizaki et al., 2008). After 3 days of incubation, positive transformants were selected on Gamborg's B5 plates supplemented with 10 μg/ml hygromicin B (Invitrogen), 0.5 μM chlorosulfuron or kanamycin, and 100 μg/ml of cefotaxime sodium. Isogenic lines were obtained using plants derived from gemmae of the T1 generation (G1 generation). G1 or subsequent gemmae generations were used for all experiments, as they are derived from single cells (Barnes and Land, 1907; Hughes, 1971). Transformation of *A. thaliana* via *A. tumefaciens* (GV3101) was performed by floral dipping according to the method of Bent (2006). Primers used for amplification of promoter fragments of Mp*FER* are listed in Table S2.

Microscopy

Plants were observed in a Lumar.V12 (ZEISS) or a Leica MZFLIII dissection microscope and imaged with an Axiocam HRc (ZEISS) or Leica DFC 420C camera. Clearings were observed using a Leica DMR microscope and photographed with an Axiocam 105 color camera. Fluorescence reporter expression was analyzed using a Leica SP5 confocal microscope. Fiji (Schindelin et al., 2012) and GIMP (version 2.8.10) software were used for adjustments of brightness, contrast, channel selection and image size.

Tissue clearing for brightfield microscopy

M. polymorpha tissues were fixed in Carnoy's solution and incubated at 4°C overnight, followed by rehydration in an ethanol (EtOH) series of 85%, 70%, 50% and 30%. Samples were incubated for 1 h at 4°C for each step and then incubated in chloral hydrate solution at 4°C overnight. Samples were mounted in chloral hydrate.

Calcofluor White staining for cell size measurements

Pieces of fresh thallus tissue located in fully differentiated zones (Solly et al., 2017) of plants grown on plates were dissected out and put into water. The pieces were transferred to PBS pH 6.1 containing 100 μg/ml Calcofluor White and vacuum-infiltrated for 1 h before being mounted on slides. The area of the epidermal cells was measured using Imaris 8.3.1. software (Bitplane AG). Cells of air pores and the two adjacent cell layers were excluded from the analysis, as well as the spiraling cells surrounding newly developing air pores.

Cell death staining

Seven-day-old gemmalings were stained with lactophenol-Trypan Blue (10 ml of lactic acid, 10 ml of glycerol, 10 g of phenol, 10 mg of Trypan Blue, dissolved in 10 ml of distilled water) by boiling them for approximately 1 min in the stain solution and then decolorized in chloral hydrate (2.5 g of chloral hydrate dissolved in 1 ml of distilled water) for at least 30 min. They were mounted in chloral hydrate and imaged using a dissection microscope.

Scanning electron microscopy

Twenty-day-old plants of wild type and $_{pro}$Mp*EF1:*Mp*FER-Cit* lines #5 and #9 were harvested and fixed in glutaraldehyde (0.25% in 20 mM HEPES) overnight at 4°C. After fixation, dehydration with an acetone series (from 50% to 100% acetone 'ultradry') was carried out. The samples were then critical-point dried, without the following sputter-coating step. Microscopic imaging was performed on a JSM-6010 scanning electron microscope (JEOL) at the Center for Microscopy and Image Analysis at the University of Zurich.

Cellular force microscopy

To evaluate the stiffness of the gemmaling tissue, we used cellular force microscopy (Felekis et al., 2011; Vogler et al., 2013). A microelectromechanical systems (MEMS)-based FT-S100 force sensor (FemtoTools AG) with a glued-on tungsten probe (T-4-22; Picoprobe by GGB Industries) was used to indent the gemmaling tissue. The sensor has a force range of ±100 µN and a resolution of 15 nN measured at 500 Hz. The sensor was attached with a custom-made acrylic arm to an *xyz* positioner (SLC-2460-M, SmarAct), which was fixed on an *xyz* piezo stage (P-563.3CD PIMars; Physik Instrumente). The *xyz* positioner was used for the rough positioning of the sensor on a part of a gemma that was as much as possible in contact with the supporting glass slide and away from the meristematic zones. Nine evenly spaced measurements were then taken in a 3×3 grid, again using the *xyz* positioner to place the sensor, while the indentation at each position was driven by the piezo stage. This procedure was repeated a second time on each gemmaling, whenever possible on the opposite lobe.

The stiffness analysis was achieved with MATLAB (MathWorks) based on the slope fitted to the force-displacement curves, which were acquired by cellular force microscopy. In a first round of data curation, each force-indentation curve was visually inspected, and curves that did not have a clear contact point or showed a clear displacement of the gemmaling, indicated by an irregular slope, were discarded. The remaining data exhibited a bimodal distribution with a high density at very soft values around 1 µN, indicating the presence of an artifact due to gemmalings that were not in contact with the slide and, therefore, were displaced rather than indented. To identify such failed measurements, we pooled all data and fitted a Gaussian mixture model with two components. We then removed all measurements that were closer than three standard deviations to the mean of the distribution with the smallest mean (mean=1.16 µN and s.d.=0.56 µN). Hence, all measurements with a value below 2.9 µN were removed.

Boxplots and statistical analysis were performed in MATLAB. The statistical tests used to assess the significance of differences between groups are indicated in the figure legends.

Western blot analysis

M. polymorpha explants were ground in liquid nitrogen and resuspended in 300 µl of Laemmli buffer (Laemmli, 1970). After centrifugation at 6000 rpm (3800 **g**) for 5 min at 4°C, the supernatant was recovered. Protein accumulation was confirmed by western blotting using an anti-GFP antibody (1:3000; TP401, Torrey Pines Biolabs). As secondary antibody, a goat anti-rabbit antibody (1:20,000; S09602, Agrisera) was used followed by ECL detection using the FUSION FX - Western Blot & Chemi Imaging system (Vilber Lourmat).

Growth rate experiments

Gemmae of wild-type, Mp*fer-1* and independent transformation lines of amiR-Mp*FER* lines were grown on plates and the thallus area was measured

over time. Ten or 30 gemmae of four independent transformation lines were grown on half-strength Gamborg's B5 and scanned on an Epson 2450 Photo scanner at 600 dpi. Plant area was measured using color threshold settings and particle analysis in Fiji software (Schindelin et al., 2012).

Expression map

Gene expression of *Cr*RLK1L signaling pathway components was calculated from publicly available RNA-seq data of 39 samples of *M. polymorpha* Tak-1 and Tak-2. Samples were grouped by tissue and analyzed under the same pipeline: Nextera paired-end adapters were trimmed from sequencing reads using the bbduk tool embedded in the BBMap software package (Bushnell, 2014). Read ends with quality below 20 were also trimmed and the minimum read length was set to 25. The rest of parameters of bbduk were set at default values. Reads were mapped to *M. polymorpha* reference genome (v3.1) (Bowman et al., 2017) using the TopHat software (v2.1.1) (Trapnell et al., 2009), designed for RNA-sequencing read mapping. TopHat contains Bowtie (v2.3.2.0) (Langdon, 2015) as the aligner software. All parameters were set to default values except for the RAM memory and number of used Cores. Mapped reads were sorted using samtools (v1.3.1) (Li et al., 2009) and counted with the software HTSeq-count (v.0.9.1) (Anders et al., 2015). Gene expression values were calculated using the package DESeq2 (Release 3.6) (Love et al., 2014) for R software (v3.4.4) (https://www.R-project.org/). Another R package, ggplot2 (release 2.2.1) (Wickham, 2016), was used for producing the figures. A summary of the samples that were used in this study is provided in Table S3.

Chlorophyll efflux rate

To measure the chlorophyll efflux rate (Lolle et al., 1997), 10-day-old gemmalings were used. Sixteen replicates of MpFER-overexpressor, Mp*fer-2* mutant, and wild-type lines were immersed in an 80% EtOH solution in 5-ml tubes. The tubes were agitated gently on a shaker platform. Aliquots of 2 µl were removed every minute, during the first 10 min. The amount of chlorophyll extracted by the EtOH solution was quantified with a spectrophotometer (NanoDrop 8000, Thermo Fisher Scientific) and calculated from UV light absorption at 647 and 664 nm. The micromolar concentration of total chlorophyll per gram of fresh weight of tissue per ml of EtOH was calculated using the following equation: total micromoles chlorophyll=$7.93(A_{664})+19.53(A_{647})$.

3D protein structure modeling

Comparative modeling of protein 3D structures was performed using the SWISS-MODEL online tool (Schwede et al., 2003). The software was fed with the three protein sequences of MpFER, MpRALF1 and MpLRE1 as input to model. The templates chosen for modeling the three sequences were selected from the best homology result provided by SWISS-MODEL (Table S4). Quality control of the model was assessed using the same tool and the results are summarized in Table S4. Spatial comparisons of the *M. polymorpha* predicted structures with the crystal structures of *A. thaliana* were performed in PyMOL (DeLano, 2002).

Quantification and statistical analysis

Analyses were performed in InfoStat (http://www.infostat.com.ar), the R base package and MATLAB. Statistical tests are indicated in the corresponding figure legend.

Competing interests

The authors declare no competing or financial interests.

References

Aach, J., Mali, P. and Church, G. M. (2014). CasFinder: flexible algorithm for identifying specific Cas9 targets in genomes. *bioRxiv* doi:10.1101/005074

Althoff, F., Kopischke, S., Zobell, O., Ide, K., Ishizaki, K., Kohchi, T. and Zachgo, S. (2014). Comparison of the Mp*EF1α* and CaMV35 promoters for application in *Marchantia polymorpha* overexpression studies. *Transgenic Res.* **23**, 235-244. doi:10.1007/s11248-013-9746-z

Anders, S., Pyl, P. T. and Huber, W. (2015). HTSeq – a Python framework to work with high-throughput sequencing data. *Bioinformatics* **31**, 166-169. doi:10.1093/bioinformatics/btu638

Bai, L., Ma, X., Zhang, G., Song, S., Zhou, Y., Gao, L., Miao, Y. and Song, C.-P. (2014). A receptor-like kinase mediates ammonium homeostasis and is important for the polar growth of root hairs in *Arabidopsis*. *Plant Cell* **26**, 1497-1511. doi:10.1105/tpc.114.124586

Barnes, C. R. and Land, W. J. G. (1907). Bryological papers. I. The origin of air chambers. *Bot Gaz* **44**, 197-213. doi:10.1086/329317

Baumberger, N., Ringli, C. and Keller, B. (2001). The chimeric leucine-rich repeat/extensin cell wall protein LRX1 is required for root hair morphogenesis in *Arabidopsis thaliana*. *Genes Dev.* **15**, 1128-1139. doi:10.1101/gad.200201

Bent, A. (2006). *Agrobacterium Protocols*. Vol. I, 2nd edn. Totowa, NJ: Humana Press.

Boisson-Dernier, A., Roy, S., Kritsas, K., Grobei, M. A., Jaciubek, M., Schroeder, J. I. and Grossniklaus, U. (2009). Disruption of the pollen-expressed *FERONIA* homologs *ANXUR1* and *ANXUR2* triggers pollen tube discharge. *Development* **136**, 3279-3288. doi:10.1242/dev.040071

Boisson-Dernier, A., Kessler, S. A. and Grossniklaus, U. (2011). The walls have ears: the role of plant *Cr*RLK1Ls in sensing and transducing extracellular signals. *J. Exp. Bot.* **62**, 1581-1591. doi:10.1093/jxb/erq445

Boisson-Dernier, A., Franck, C. M., Lituiev, D. S. and Grossniklaus, U. (2015). Receptor-like cytoplasmic kinase MARIS functions downstream of *Cr*RLK1L-dependent signaling during tip growth. *Proc. Natl. Acad. Sci. USA* **112**, 12211-12216. doi:10.1073/pnas.1512375112

Bouton, S., Leboeuf, E., Mouille, G., Leydecker, M.-T., Talbotec, J., Granier, F., Lahaye, M., Höfte, H. and Truong, H.-N. (2002). *QUASIMODO1* encodes a putative membrane-bound glycosyltransferase required for normal pectin synthesis and cell adhesion in *Arabidopsis*. *Plant Cell* **14**, 2577-2590. doi:10.1105/tpc.004259

Bowen, E. J. (1935). A note on the conduction of water in *Fimbriaria bleumeana*. *Ann. Bot.* **49**, 844-848. doi:10.1093/oxfordjournals.aob.a090540

Bowman, J. L., Floyd, S. K. and Sakakibara, K. (2007). Green genes-comparative genomics of the green branch of life. *Cell* **129**, 229-234. doi:10.1016/j.cell.2007.04.004

Bowman, J. L., Araki, T., Arteaga-Vazquez, M. A., Berger, F., Dolan, L., Haseloff, J., Ishizaki, K., Kyozuka, J., Lin, S.-S., Nagasaki, H., et al. (2016). The naming of names: guidelines for gene nomenclature in *Marchantia*. *Plant Cell Physiol.* **57**, 257-261. doi:10.1093/pcp/pcv193

Bowman, J. L., Kohchi, T., Yamato, K. T., Jenkins, J., Shu, S., Ishizaki, K., Yamaoka, S., Nishihama, R., Nakamura, Y., Berger, F. et al. (2017). Insights into land plant evolution garnered from the *Marchantia polymorpha* genome. *Cell* **171**, 287-304.e15. doi:10.1016/j.cell.2017.09.030

Bushnell, B. (2014). *BBMap: a fast, accurate, splice-aware aligner (No. LBNL-7065E)*. Berkeley, CA, US: Lawrence Berkeley Natl. LabLBNL.

Capron, A., Gourgues, M., Neiva, L. S., Faure, J.-E., Berger, F., Pagnussat, G., Krishnan, A., Alvarez-Mejia, C., Vielle-Calzada, J.-P., Lee, Y.-R., et al. (2008). Maternal control of male-gamete delivery in *Arabidopsis* involves a putative GPI-anchored protein encoded by the *LORELEI* gene. *Plant Cell* **20**, 3038-3049. doi:10.1105/tpc.108.061713

Cheung, A. Y. and Wu, H.-M. (2011). THESEUS 1, FERONIA and relatives: a family of cell wall-sensing receptor kinases? *Curr. Opin. Plant Biol.* **14**, 632-641. doi:10.1016/j.pbi.2011.09.001

Chiyoda, S., Ishizaki, K., Kataoka, H., Yamato, K. T. and Kohchi, T. (2008). Direct transformation of the liverwort *Marchantia polymorpha* L. by particle bombardment using immature thalli developing from spores. *Plant Cell Rep.* **27**, 1467-1473. doi:10.1007/s00299-008-0570-5

Curtis, M. D. and Grossniklaus, U. (2003). A Gateway cloning vector set for high-throughput functional analysis of genes *in planta*. *Plant Physiol.* **133**, 462-469. doi:10.1104/pp.103.027979

De Rybel, B., van den Berg, W., Lokerse, A. S., Liao, C.-Y., van Mourik, H., Möller, B., Llavata-Peris, C. I. and Weijers, D. (2011). A versatile set of ligation-independent cloning vectors for functional studies in plants. *Plant Physiol.* **156**, 1292-1299. doi:10.1104/pp.111.177337

DeLano, W. L. (2002). Pymol: an open-source molecular graphics tool. *CCP4 Newsl. Protein Crystallogr.* **40**, 82-92.

Denness, L., McKenna, J. F., Segonzac, C., Wormit, A., Madhou, P., Bennett, M., Mansfield, J., Zipfel, C. and Hamann, T. (2011). Cell wall damage-induced lignin biosynthesis is regulated by a reactive oxygen species- and jasmonic acid-dependent process in *Arabidopsis*. *Plant Physiol.* **156**, 1367-1374. doi:10.1104/pp.111.175737

Deslauriers, S. D. and Larsen, P. B. (2010). FERONIA is a key modulator of brassinosteroid and ethylene responsiveness in *Arabidopsis* hypocotyls. *Mol. Plant* **3**, 626-640. doi:10.1093/mp/ssq015

Duan, Q., Kita, D., Li, C., Cheung, A. Y. and Wu, H.-M. (2010). FERONIA receptor-like kinase regulates RHO GTPase signaling of root hair development. *Proc. Natl. Acad. Sci. USA* **107**, 17821-17826. doi:10.1073/pnas.1005366107

Dünser, K., Gupta, S., Herger, A., Feraru, M. I., Ringli, C. and Kleine-Vehn, J. (2019). Extracellular matrix sensing by FERONIA and Leucine-Rich Repeat Extensins controls vacuolar expansion during cellular elongation in *Arabidopsis thaliana*. *EMBO J.* **38**, e100353. doi:10.15252/embj.2018100353

Escobar-Restrepo, J.-M., Huck, N., Kessler, S., Gagliardini, V., Gheyselinck, J., Yang, W.-C. and Grossniklaus, U. (2007). The FERONIA receptor-like kinase mediates male-female interactions during pollen tube reception. *Science* **317**, 656-660. doi:10.1126/science.1143562

Felekis, D., Muntwyler, S., Vogler, H., Beyeler, F., Grossniklaus, U. and Nelson, B. J. (2011). Quantifying growth mechanics of living, growing plant cells *in situ* using microrobotics. *Micro Nano Lett.* **6**, 311-316. doi:10.1049/mnl.2011.0024

Feng, W., Kita, D., Peaucelle, A., Cartwright, H. N., Doan, V., Duan, Q., Liu, M.-C., Maman, J., Steinhorst, L., Schmitz-Thom, I., et al. (2018). The FERONIA receptor kinase maintains cell-wall integrity during salt stress through Ca^{2+} signaling. *Curr. Biol.* **28**, 666-675.e5. doi:10.1016/j.cub.2018.01.023

Flores-Sandoval, E., Eklund, D. M. and Bowman, J. L. (2015). A simple auxin transcriptional response system regulates multiple morphogenetic processes in the liverwort *Marchantia polymorpha*. *PLoS Genet.* **11**, e1005207. doi:10.1371/journal.pgen.1005207

Flores-Sandoval, E., Dierschke, T., Fisher, T. J. and Bowman, J. L. (2016). Efficient and inducible use of artificial microRNAs in *Marchantia polymorpha*. *Plant Cell Physiol.* **57**, 281-290. doi:10.1093/pcp/pcv068

Floyd, S. K. and Bowman, J. L. (2007). The ancestral developmental tool kit of land plants. *Int. J. Plant Sci.* **168**, 1-35. doi:10.1086/509079

Franck, C. M., Westermann, J. and Boisson-Dernier, A. (2018). Plant malectin-like receptor kinases: from cell wall integrity to immunity and beyond. *Annu. Rev. Plant Biol.* **69**, 301-328. doi:10.1146/annurev-arplant-042817-040557

Fujikura, U., Elsaesser, L., Breuninger, H., Sánchez-Rodríguez, C., Ivakov, A., Laux, T., Findlay, K., Persson, S. and Lenhard, M. (2014). Atkinesin-13A modulates cell-wall synthesis and cell expansion in *Arabidopsis thaliana* via the *THESEUS1* pathway. *PLoS Genet.* **10**, e1004627. doi:10.1371/journal.pgen.1004627

Gachomo, E. W., Jno Baptiste, L., Kefela, T., Saidel, W. M. and Kotchoni, S. O. (2014). The *Arabidopsis CURVY1* (*CVY1*) gene encoding a novel receptor-like protein kinase regulates cell morphogenesis, flowering time and seed production. *BMC Plant Biol.* **14**, 221. doi:10.1186/s12870-014-0221-7

Galindo-Trigo, S., Gray, J. E. and Smith, L. M. (2016). Conserved roles of *Cr*RLK1L receptor-like kinases in cell expansion and reproduction from Algae to Angiosperms. *Front. Plant Sci.* **7**, 1269. doi:10.3389/fpls.2016.01269

Galindo-Trigo, S., Blanco-Touriñán, N., DeFalco, T. A., Wells, E. S., Gray, J. E., Zipfel, C. and Smith, L. M. (2020). *Cr*RLK1L receptor-like kinases HERK1 and ANJEA are female determinants of pollen tube reception. *EMBO Rep.* **21**, e48466. doi:10.15252/embr.201948466

Ge, Z., Bergonci, T., Zhao, Y., Zou, Y., Du, S., Liu, M.-C., Luo, X., Ruan, H., García-Valencia, L. E., Zhong, S. et al. (2017). *Arabidopsis* pollen tube integrity and sperm release are regulated by RALF-mediated signaling. *Science* **358**, 1596-1600. doi:10.1126/science.aao3642

Ginanjar, E. F., Teh, O.-K. and Fujita, T. (2021). Characterisation of rapid alkalinisation factors in *Physcomitrium patens* reveals functional conservation in tip growth. *New Phytol.* **233**, 2442-2457. doi:10.1111/nph.17942.

Gonneau, M., Desprez, T., Martin, M., Doblas, V. G., Bacete, L., Miart, F., Sormani, R., Hématy, K., Renou, J., Landrein, B. et al. (2018). Receptor kinase

DEVELOPMENT

THESEUS1 is a RAPID ALKALINIZATION FACTOR34 receptor in *Arabidopsis*. *Curr. Biol.* **28**, 2452-2458.e4. doi:10.1016/j.cub.2018.05.075

Guo, H., Li, L., Ye, H., Yu, X., Algreen, A. and Yin, Y. (2009a). Three related receptor-like kinases are required for optimal cell elongation in *Arabidopsis thaliana*. *Proc. Natl. Acad. Sci. USA* **106**, 7648-7653. doi:10.1073/pnas. 0812346106

Guo, H., Ye, H., Li, L. and Yin, Y. (2009b). A family of receptor-like kinases are regulated by BES1 and involved in plant growth in *Arabidopsis thaliana*. *Plant Signal. Behav.* **4**, 784-786. doi:10.4161/psb.4.8.9231

Haruta, M., Sabat, G., Stecker, K., Minkoff, B. B. and Sussman, M. R. (2014). A peptide hormone and its receptor protein kinase regulate plant cell expansion. *Science* **343**, 408-411. doi:10.1126/science.1244454

Hématy, K. and Höfte, H. (2008). Novel receptor kinases involved in growth regulation. *Curr. Opin. Plant Biol.* **11**, 321-328. doi:10.1016/j.pbi.2008.02.008

Hématy, K., Sado, P.-E., Van Tuinen, A., Rochange, S., Desnos, T., Balzergue, S., Pelletier, S., Renou, J.-P. and Höfte, H. (2007). A receptor-like kinase mediates the response of *Arabidopsis* cells to the inhibition of cellulose synthesis. *Curr. Biol.* **17**, 922-931. doi:10.1016/j.cub.2007.05.018

Hirano, N., Marukawa, Y., Abe, J., Hashiba, S., Ichikawa, M., Tanabe, Y., Ito, M., Nishii, I., Tsuchikane, Y. and Sekimoto, H. (2015). A Receptor-like kinase, related to cell wall sensor of higher plants, is required for sexual reproduction in the unicellular Charophycean alga, *Closterium peracerosum–strigosum–littorale* complex. *Plant Cell Physiol.* **56**, 1456-1462. doi:10.1093/pcp/pcv065

Honkanen, S., Jones, V. A. S., Morieri, G., Champion, C., Hetherington, A. J., Kelly, S., Proust, H., Saint-Marcoux, D., Prescott, H. and Dolan, L. (2016). The mechanism forming the cell surface of tip-growing rooting cells is conserved among land plants. *Curr. Biol.* **26**, 3238-3244. doi:10.1016/j.cub.2016.09.062

Huck, N., Moore, J. M., Federer, M. and Grossniklaus, U. (2003). The *Arabidopsis* mutant *feronia* disrupts the female gametophytic control of pollen tube reception. *Development* **130**, 2149-2159. doi:10.1242/dev.00458

Hughes, S. J. (1971). On conidia of fungi, and gemmae of algae, bryophytes, and pteridophytes. *Can. J. Bot.* **49**, 1319-1339. doi:10.1139/b71-187

Humplík, J. F., Bergougnoux, V. and Van Volkenburgh, E. (2017). To stimulate or inhibit? That is the question for the function of abscisic acid. *Trends Plant Sci.* **22**, 830-841. doi:10.1016/j.tplants.2017.07.009

Ishizaki, K. (2017). Evolution of land plants: insights from molecular studies on basal lineages. *Biosci. Biotechnol. Biochem.* **81**, 73-80. doi:10.1080/09168451. 2016.1224641

Ishizaki, K., Chiyoda, S., Yamato, K. T. and Kohchi, T. (2008). *Agrobacterium*-mediated transformation of the haploid liverwort *Marchantia polymorpha* L., an emerging model for plant biology. *Plant Cell Physiol.* **49**, 1084-1091. doi:10.1093/ pcp/pcn085

Ishizaki, K., Nishihama, R., Ueda, M., Inoue, K., Ishida, S., Nishimura, Y., Shikanai, T. and Kohchi, T. (2015). Development of gateway binary vector series with four different selection markers for the liverwort *Marchantia polymorpha*. *PLoS ONE* **10**, e0138876. doi:10.1371/journal.pone.0138876

Keinath, N. F., Kierszniowska, S., Lorek, J., Bourdais, G., Kessler, S. A., Shimosato-Asano, H., Grossniklaus, U., Schulze, W. X., Robatzek, S. and Panstruga, R. J. (2010). PAMP (pathogen-associated molecular pattern)-induced changes in plasma membrane compartmentalization reveal novel components of plant immunity. *J. Biol. Chem.* **285**, 39140-39149. doi:10.1074/ jbc.M110.160531

Kenrick, P. and Crane, P. R. (1997). The origin and early evolution of plants on land. *Nature* **389**, 33-39. doi:10.1038/37918

Kessler, S. A., Shimosato-Asano, H., Keinath, N. F., Wuest, S. E., Ingram, G., Panstruga, R. and Grossniklaus, U. (2010). Conserved molecular components for pollen tube reception and fungal invasion. *Science* **330**, 968-971. doi:10.1126/ science.1195211

Kessler, S. A., Lindner, H., Jones, D. S. and Grossniklaus, U. (2014). Functional analysis of related *Cr*RLK1L receptor-like kinases in pollen tube reception. *EMBO Rep.* **16**, 107-115. doi:10.15252/embr.201438801

Kim, C. M. and Dolan, L. (2016). *ROOT HAIR DEFECTIVE SIX-LIKE* class I genes promote root hair development in the grass *Brachypodium distachyon*. *PLoS Genet.* **12**, e1006211. doi:10.1371/journal.pgen.1006211

Kubota, A., Ishizaki, K., Hosaka, M. and Kohchi, T. (2013). Efficient *Agrobacterium*-mediated transformation of the liverwort *Marchantia polymorpha* using regenerating thalli. *Biosci. Biotechnol. Biochem.* **77**, 167-172. doi:10.1271/ bbb.120700

Laemmli, U. K. (1970). Cleavage of structural proteins during the assembly of the head of bacteriophage T4. *Nature* **227**, 680-685. doi:10.1038/227680a0

Langdon, W. B. (2015). Performance of genetic programming optimised Bowtie2 on genome comparison and analytic testing (GCAT) benchmarks. *BioData Min.* **8**, 1. doi:10.1186/s13040-014-0034-0

Li, H., Handsaker, B., Wysoker, A., Fennell, T., Ruan, J., Homer, N., Marth, G., Abecasis, G. and Durbin, R. (2009). The sequence alignment/map format and SAMtools. *Bioinformatics* **25**, 2078-2079. doi:10.1093/bioinformatics/btp352

Li, C., Yeh, F.-L., Cheung, A. Y., Duan, Q., Kita, D., Liu, M.-C., Maman, J., Luu, E. J., Wu, B. W., Gates, L. et al. (2015). Glycosylphosphatidylinositol-anchored proteins as chaperones and co-receptors for FERONIA receptor kinase signaling in *Arabidopsis*. *eLife* **4**, e06587. doi:10.7554/eLife.06587.031

Liao, H.-Z., Zhu, M.-M., Cui, H.-H., Du, X.-Y., Tang, Y., Chen, L.-Q., Ye, D. and Zhang, X.-Q. (2016). *MARIS* plays important roles in *Arabidopsis* pollen tube and root hair growth. *J. Integr. Plant Biol.* **58**, 927-940. doi:10.1111/jipb.12484

Lin, W., Tang, W., Pan, X., Huang, A., Gao, X., Anderson, C. T. and Yang, Z. (2021). *Arabidopsis* pavement cell morphogenesis requires FERONIA binding to pectin for activation of ROP GTPase signaling. *Curr. Biol.* **32**, 497-507.e4. doi:10. 1016/j.cub.2021.11.030

Lindner, H., Müller, L. M., Boisson-Dernier, A. and Grossniklaus, U. (2012). *Cr*RLK1L receptor-like kinases: not just another brick in the wall. *Curr. Opin. Plant Biol.* **15**, 659-669. doi:10.1016/j.pbi.2012.07.003

Liu, L., Zheng, C., Kuang, B., Wei, L., Yan, L. and Wang, T. (2016). Receptor-like kinase RUPO interacts with potassium transporters to regulate pollen tube growth and integrity in rice. *PLoS Genet.* **12**, e1006085. doi:10.1371/journal.pgen. 1006085

Lolle, S. J., Berlyn, G. P., Engstrom, E. M., Krolikowski, K. A., Reiter, W.-D. and Pruitt, R. E. (1997). Developmental regulation of cell interactions in the *Arabidopsis fiddlehead-1* mutant: a role for the epidermal cell wall and cuticle. *Dev. Biol.* **189**, 311-321. doi:10.1006/dbio.1997.8671

Love, M. I., Huber, W. and Anders, S. (2014). Moderated estimation of fold change and dispersion for RNA-seq data with DESeq2. *Genome Biol.* **15**, 550. doi:10. 1186/s13059-014-0550-8

Malivert, A., Erguvan, Ö., Chevallier, A., Dehem, A., Friaud, R., Liu, M., Martin, M., Peyraud, T., Hamant, O. and Verger, S. (2021). *FERONIA* and microtubules independently contribute to mechanical integrity in the *Arabidopsis* shoot. *PLoS Biol.* **19**, e3001454. doi:10.1371/journal.pbio.3001454

Mao, D., Yu, F., Li, J., Van de Poel, B., Tan, D., Li, J., Liu, Y., Li, X., Dong, M., Chen, L. et al. (2015). FERONIA receptor kinase interacts with S-adenosylmethionine synthetase and suppresses S-adenosylmethionine production and ethylene biosynthesis in *Arabidopsis*. *Plant Cell Env.* **38**, 2566-2574. doi:10.1111/pce.12570

Mecchia, M. A., Santos-Fernandez, G., Duss, N. N., Somoza, S. C., Boisson-Dernier, A., Gagliardini, V., Martínez-Bernardini, A., Fabrice, T. N., Ringli, C., Muschietti, J. P. et al. (2017). RALF4/19 peptides interact with LRX proteins to control pollen tube growth in *Arabidopsis*. *Science* **358**, 1600-1603. doi:10.1126/ science.aao5467

Merz, D., Richter, J., Gonneau, M., Sanchez-Rodriguez, C., Eder, T., Sormani, R., Martin, M., Hématy, K., Höfte, H. and Hauser, M.-T. (2017). T-DNA alleles of the receptor kinase THESEUS1 with opposing effects on cell wall integrity signaling. *J. Exp. Bot.* **68**, 4583-4593. doi:10.1093/jxb/erx263

Mishler, B. D. and Churchill, S. P. (1984). A cladistic approach to the phylogeny of the 'bryophytes'. *Brittonia* **36**, 406-424. doi:10.2307/2806602

Miyazaki, S., Murata, T., Sakurai-Ozato, N., Kubo, M., Demura, T., Fukuda, H. and Hasebe, M. (2009). *ANXUR1* and *2*, sister genes to *FERONIA*/*SIRENE*, are male factors for coordinated fertilization. *Curr. Biol.* **19**, 1327-1331. doi:10.1016/j. cub.2009.06.064

Ngo, Q. A., Vogler, H., Lituiev, D. S., Nestorova, A. and Grossniklaus, U. (2014). A calcium dialog mediated by the *FERONIA* signal transduction pathway controls plant sperm delivery. *Dev. Cell* **29**, 491-500. doi:10.1016/j.devcel.2014.04.008

Nishiyama, T., Fujita, T., Shin-I, T., Seki, M., Nishide, H., Uchiyama, I., Kamiya, A., Carninci, P., Hayashizaki, Y., Shinozaki, K. et al. (2003). Comparative genomics of *Physcomitrella patens* gametophytic transcriptome and *Arabidopsis thaliana*: implication for land plant evolution. *Proc. Natl. Acad. Sci. USA* **100**, 8007-8012. doi:10.1073/pnas.0932694100

Nissen, K. S., Willats, W. G. T. and Malinovsky, F. G. (2016). Understanding *Cr*RLK1L function: cell walls and growth control. *Trends Plant Sci.* **21**, 516-527. doi:10.1016/j.tplants.2015.12.004

Okuda, S., Tsutsui, H., Shiina, K., Sprunck, S., Takeuchi, H., Yui, R., Kasahara, R. D., Hamamura, Y., Mizukami, A., Susaki, D., et al. (2009). Defensin-like polypeptide LUREs are pollen tube attractants secreted from synergid cells. *Nature* **458**, 357-361. doi:10.1038/nature07882

Pierik, R., Tholen, D., Poorter, H., Visser, E. J. W. and Voesenek, L. A. (2006). The Janus face of ethylene: growth inhibition and stimulation. *Trends Plant Sci.* **11**, 176-183. doi:10.1016/j.tplants.2006.02.006

Qiu, Y.-L., Li, L., Wang, B., Chen, Z., Knoop, V., Groth-Malonek, M., Dombrovska, O., Lee, J., Kent, L., Rest, J. et al. (2006). The deepest divergences in land plants inferred from phylogenomic evidence. *Proc. Natl. Acad. Sci. USA* **103**, 15511-15516. doi:10.1073/pnas.0603335103

Richter, J., Ploderer, M., Mongelard, G., Gutierrez, L. and Hauser, M.-T. (2017). Role of *Cr*RLK1L cell wall sensors HERCULES1 and 2, THESEUS1, and FERONIA in growth adaptation triggered by heavy metals and trace elements. *Front. Plant Sci.* **8**, 1554. doi:10.3389/fpls.2017.01554

Richter, J., Watson, J. M., Stasnik, P., Borowska, M., Neuhold, J., Berger, M., Stolt-Bergner, P., Schoft, V. and Hauser, M.-T. (2018). Multiplex mutagenesis of four clustered *Cr*RLK1L with CRISPR/Cas9 exposes their growth regulatory roles in response to metal ions. *Sci. Rep.* **8**, 12182. doi:10.1038/s41598-018-30711-3

Rotman, N., Rozier, F., Boavida, L., Dumas, C., Berger, F. and Faure, J.-E. (2003). Female control of male gamete delivery during fertilization in *Arabidopsis thaliana*. *Curr. Biol.* **13**, 432-436. doi:10.1016/S0960-9822(03)00093-9

Rövekamp, M., Bowman, J. L. and Grossniklaus, U. (2014). Back to the rhizoids of plant sexual development. *23rd Int. Congr. Sex. Plant Reprod. Porto*

Port., p. 132. https://www.fc.up.pt/sprporto2014/doc/23rd%20International%20congress%20on%20sexual%20plant%20reproduction%20ABSBook.pdf.

Rövekamp, M., Bowman, J. L. and Grossniklaus, U. (2016). *Marchantia* MpRKD regulates the gametophyte-sporophyte transition by keeping egg cells quiescent in the absence of fertilization. *Curr. Biol.* **26**, 1782-1789. doi:10.1016/j.cub.2016.05.028

Sachs, A. B. and Varani, G. (2000). Eukaryotic translation initiation: there are (at least) two sides to every story. *Nat. Struct. Biol.* **7**, 356-361. doi:10.1038/75120

Schindelin, J., Arganda-Carreras, I., Frise, E., Kaynig, V., Longair, M., Pietzsch, T., Preibisch, S., Rueden, C., Saalfeld, S., Schmid, B. et al. (2012). Fiji: An open-source platform for biological-image analysis. *Nat. Methods* **9**, 676-682. doi:10.1038/nmeth.2019

Schoenaers, S., Balcerowicz, D., Breen, G., Hill, K., Zdanio, M., Mouille, G., Holman, T. J., Oh, J., Wilson, M. H., Nikonorova, N. et al. (2018). The auxin-regulated *Cr*RLK1L kinase ERULUS controls cell wall composition during root hair tip growth. *Curr. Biol.* **28**, 722-732. doi:10.1016/j.cub.2018.01.050

Schulze-Muth, P., Irmler, S., Schröder, G. and Schröder, J. (1996). Novel type of receptor-like protein kinase from a higher plant (*Catharanthus roseus*): cDNA, gene, intramolecular autophosphorylation, and identification of a threonine important for auto- and substrate phosphorylation. *J. Biol. Chem.* **271**, 26684-26689. doi:10.1074/jbc.271.43.26684

Schwede, T., Kopp, J., Guex, N. and Peitsch, M. C. (2003). SWISS-MODEL: an automated protein homology-modeling server. *Nucleic Acids Res.* **31**, 3381-3385. doi:10.1093/nar/gkg520

Shih, H.-W., Miller, N. D., Dai, C., Spalding, E. P. and Monshausen, G. B. (2014). The receptor-like kinase FERONIA is required for mechanical signal transduction in *Arabidopsis* seedlings. *Curr. Biol.* **24**, 1887-1892. doi:10.1016/j.cub.2014.06.064

Shiu, S. H. and Bleecker, A. B. (2001). Plant receptor-like kinase gene family: diversity, function, and signaling. *Sci. STKE* **2001**, re22. doi:10.1126/stke.2001.113.re22

Showalter, A. M. (1993). Structure and function of plant cell wall proteins. *Plant Cell* **5**, 9-23. doi:10.1105/tpc.5.1.9

Solly, J. E., Cunniffe, N. J. and Harrison, C. J. (2017). Regional growth rate differences specified by apical notch activities regulate liverwort thallus shape. *Curr. Biol.* **27**, 16-26. doi:10.1016/j.cub.2016.10.056

Srivastava, R., Liu, J.-X., Guo, H., Yin, Y. and Howell, S. H. (2009). Regulation and processing of a plant peptide hormone, AtRALF23, in *Arabidopsis*. *Plant J.* **59**, 930-939. doi:10.1111/j.1365-313X.2009.03926.x

Stegmann, M., Monaghan, J., Smakowska-Luzan, E., Rovenich, H., Lehner, A., Holton, N., Belkhadir, Y. and Zipfel, C. (2017). The receptor kinase FER is a RALF-regulated scaffold controlling plant immune signaling. *Science* **355**, 287-289. doi:10.1126/science.aal2541

Steinwand, B. J. and Kieber, J. J. (2010). The role of receptor-like kinases in regulating cell wall function. *Plant Physiol.* **153**, 479-484. doi:10.1104/pp.110.155887

Tang, W., Lin, W., Zhou, X., Guo, J., Dang, X., Li, B., Lin, D. and Yang, Z. (2021). Mechano-transduction via the pectin-FERONIA complex activates ROP6 GTPase signaling in *Arabidopsis* pavement cell morphogenesis. *Curr. Biol.* **S0960-9822**, 01590-01596.

Trapnell, C., Pachter, L. and Salzberg, S. L. (2009). TopHat: discovering splice junctions with RNA-Seq. *Bioinformatics* **25**, 1105-1111. doi:10.1093/bioinformatics/btp120

Vandesompele, J., De Preter, K., Pattyn, F., Poppe, B., Van Roy, N., De Paepe, A. and Speleman, F. (2002). Accurate normalization of real-time quantitative RT-PCR data by geometric averaging of multiple internal control genes. *Genome Biol.* **3**, RESEARCH0034. doi:10.1186/gb-2002-3-7-research0034

Vogler, H., Draeger, C., Weber, A., Felekis, D., Eichenberger, C., Routier-Kierzkowska, A.-L., Boisson-Dernier, A., Ringli, C., Nelson, B. J., Smith, R. S., et al. (2013). The pollen tube: a soft shell with a hard core. *Plant J.* **73**, 617-627. doi:10.1111/tpj.12061

Westermann, J., Streubel, S., Franck, C. M., Lentz, R., Dolan, L. and Boisson-Dernier, A. (2019). An evolutionarily conserved receptor-like kinases signaling module controls cell wall integrity during tip growth. *Curr. Biol.* **29**, 4153. doi:10.1016/j.cub.2019.11.010

Wickett, N. J., Mirarab, S., Nguyen, N., Warnow, T., Carpenter, E., Matasci, N., Ayyampalayam, S., Barker, M. S., Burleigh, J. G., Gitzendanner, M. A. et al. (2014). Phylotranscriptomic analysis of the origin and early diversification of land plants. *Proc. Natl. Acad. Sci. USA* **1111**, E4859-E4868. doi:10.1073/pnas.1323926111

Wickham, H. (2016). *ggplot2: elegant graphics for data analysis*. Springer.

Wolf, S. and Höfte, H. (2014). Growth control: a saga of cell walls, ROS, and peptide receptors. *Plant Cell* **26**, 1848-1856. doi:10.1105/tpc.114.125518

Wolf, S., Hématy, K. and Höfte, H. (2012). Growth control and cell wall signaling in plants. *Annu. Rev. Plant Biol.* **63**, 381-407. doi:10.1146/annurev-arplant-042811-105449

Xiao, Y., Stegmann, M., Han, Z., DeFalco, T. A., Parys, K., Xu, L., Belkhadir, Y., Zipfel, C. and Chai, J. (2019). Mechanisms of RALF peptide perception by a heterotypic receptor complex. *Nature* **572**, 270-274. doi:10.1038/s41586-019-1409-7

Yu, F., Qian, L., Nibau, C., Duan, Q., Kita, D., Levasseur, K., Li, X., Lu, C., Li, H., Hou, C. et al. (2012). FERONIA receptor kinase pathway suppresses abscisic acid signaling in *Arabidopsis* by activating ABI2 phosphatase. *Proc. Natl. Acad. Sci. USA* **109**, 14693-14698. doi:10.1073/pnas.1212547109

Zhu, L., Chu, L.-C., Liang, Y., Zhang, X.-Q., Chen, L.-Q. and Ye, D. (2018). The *Arabidopsis Cr*RLK1L protein kinases BUPS1 and BUPS2 are required for normal growth of pollen tubes in the pistil. *Plant J.* **95**, 474-486. doi:10.1111/tpj.13963

Zhu, S., Fu, Q., Xu, F., Zheng, H. and Yu, F. (2021). New paradigms in cell adaptation: decades of discoveries on the *Cr*RLK1L receptor kinase signalling network. *New Phytol.* **232**, 1168-1183. doi:10.1111/nph.17683

Zuker, M. (2003). Mfold web server for nucleic acid folding and hybridization prediction. *Nucleic Acids Res.* **31**, 3406-3415. doi:10.1093/nar/gkg595

DEVELOPMENT